DETERMINATION OF THE DYNAMIC STRENGTH OF IRON AT LOW TEMPERATURE

By

Gary T. Lockhart

B. A. Sc. University of British Columbia, 1988

A THESIS SUBMITTED IN PARTIAL FULFILLMENT OF

THE REQUIREMENTS FOR THE DEGREE OF

MASTER OF APPLIED SCIENCE

in

THE FACULTY OF GRADUATE STUDIES

METALS AND MATERIALS ENGINEERING

We accept this thesis as conforming

to the required standard

THE UNIVERSITY OF BRITISH COLUMBIA

April 1992

In presenting this thesis in partial fulfilment of the requirements for an advanced degree at the University of British Columbia, I agree that the Library shall make it freely available for reference and study. I further agree that permission for extensive copying of this thesis for scholarly purposes may be granted by the head of my department or by his or her representatives. It is understood that copying or publication of this thesis for financial gain shall not be allowed without my written permission.

(Signature) _____

Department of Metals and Materials Engineering

The University of British Columbia
Vancouver, Canada

Date April 29, 1992

DE-6 (2/88)

Abstract

Measurements of the stress sensitivity of the strain rate and of the strain *vs* stress in a titanium-doped, "interstitial free" (IF) iron were done at three temperatures, -20, -50 and -75 °C. By application of a deformation model, based on a new theory of mobile dislocation density, these measurements permit the determination of (1) the constants of the power law describing the dislocation velocity as a function of the effective stress, and (2) the mean free dislocation path, which is descriptive of parabolic strain hardening. The theory is then used to calculate the microstructural parameters which determine the inelastic strain rate and the deformation resistance as they evolve, over time, with stress, stress rate and temperature. These parameters include the mobile and network dislocation densities, dislocation velocity, and effective stress. Theoretical predictions of the dynamic properties show excellent agreement with experiment. These properties include: (1) the stress sensitivity of the strain rate, as influenced by stress, stress rate and the magnitude of the stress decrease; (2) the nature and recovery time of the strain rate following a stress decrease; (3) the relative level of hard machine stress *vs* strain curves as a function of crosshead speed; and (4) the temperature dependence of both the microyield and macroyield stresses.

Table of Contents

List of Tables

List of Figures

Acknowledgement

The author is grateful to Dr. T. H. Alden for his advice and direction given throughout the course of this study.

He is also grateful to fellow students for their friendship and helpful discussion, and to members of the technical and support staff – in particular, P. R. Musil for an exquisite high vacuum furnace and much improved soft tensile machine.

Further, I thank my wife, Christine Kiyomi, for her encouragement and devotion.

In presenting this thesis in partial fulfilment of the requirements for an advanced degree at the University of British Columbia, I agree that the Library shall make it freely available for reference and study. I further agree that permission for extensive copying of this thesis for scholarly purposes may be granted by the head of my department or by his or her representatives. It is understood that copying or publication of this thesis for financial gain shall not be allowed without my written permission.

N. T. Jackman

Metals and Materials Engineering
The University of British Columbia
2075 Wesbrook Place
Vancouver, Canada
V6T 1W5

Date: April 29/92

Chapter 1

Introduction

The dynamic nature of the deformation properties of metals, as indicated by the effects of temperature and deformation rate on their strength, is an important problem in the theory and practice of physical metallurgy. One problem that has received much attention over the past several decades is the strong temperature and rate dependence of the yield and flow stresses of *α-iron* at low temperature. For instance [1], the yield strength of a commercially available interstitial-free (IF) iron, pulled at a conventionally slow testing machine rate, increases 6-fold when tested at -100 °C rather than at ambient temperature. A similar, if smaller, increase in strength is also encountered at ambient temperature by increasing the strain rate to about 10^3 s^{-1} [2]. Considering that most cold forming operations are done within the range of strain rates from 10^0 to 10^3 s^{-1}, over which the yield stress for this material doubles, a prediction or interpretation of the material's strength in response to either the operating parameters of a deformation process or the external deformation variables of a mechanical test is of practical importance.

This thesis is an extension of an earlier ambient temperature investigation [3] and is an attempt to measure and to predict the dynamic properties of IF iron at three temperatures, -20, -50 and -75 °C. Although the technique in this investigation has been applied to IF iron, it is believed to have wider application and may significantly advance our quantitative understanding of inelastic deformation of other metals and alloys. In keeping with the earlier study, no attempt is made to involve a thermally-activated flow analysis, which emphasizes a precise mechanistic description of dislocation dynamics;

instead, following Johnston and Gilman [4], we obtain an empirical power law function to describe the stress dependence of the dislocation velocity. In this present work, however, this relationship is not obtained by direct observation of individual moving dislocations [4], but rather by the application, to stress sensitivity data, of a recently proposed semi-empirical model [3,5,6] purporting to describe the evolution of the mobile dislocation density.

The formulation of a quantitative theory of mobile density alone represents a significant advance in the study of dislocation dynamics, and the application of this theory differentiates this technique from all others. In principle, the equations of the theory can be used to predict various deformation behaviours since the mobile density and the dislocation velocity link to the external deformation rate through Orowan's equation $\dot{\epsilon} = \rho_m b v$. In the present study, these equations are applied to the results of an experimental study of IF iron, in which the stress is abruptly reduced by a small amount and the resulting decrease of strain rate is measured. If these tests are repeated for different applied stress rates, then stress sensitivity profiles are defined for various values of stress decrease. From a theoretical fit of such profiles, it is possible to obtain the constants of the dislocation velocity equation. When these constants have been determined, the theory permits the calculation of the dynamic strength of this material for a specified deformation rate and temperature.

1.1 The Nature of Dynamic Strength

It is an essential feature of our understanding of low temperature deformation that the strength of a solid is partly static, i.e. temperature and time independent, and partly dynamic, i.e. temperature and time dependent. The physical basis for this understanding is that the magnitude of the flow stress is determined by the interaction of mobile

dislocations with two general kinds of obstacles: (1) those possessing short range stress fields, i.e. of less than about 10 atomic diameters; or (2) those possessing long range stress fields, i.e. of the order of 10 atomic diameters or greater.

Short range obstacles are termed *thermal* obstacles because the external stress required to overcome them can be reduced by thermal fluctuations. The conventional view is that thermal fluctuations can assist the applied stress even at temperatures approaching 0 K. At 0 K, thermal activation is not possible, and the applied stress alone must release dislocations from short range obstacles. At a sufficiently high temperature, the available thermal energy may be sufficient to release dislocations with a very small (incremental) increase of the external stress above the long range (static) resistance of the solid. In this case, the obstacle is said to have become thermally transparent. Apart from these two limiting cases, the thermal release of dislocations from short range obstacles will be stress-assisted.

Besides being inherently temperature dependent, the release of dislocations from short range obstacles is a time dependent process which limits the strain rate. However, the release rate maybe enhanced by raising the external stress. Thus, in order for deformation to proceed at some imposed rate, the external stress must be increased. Conversely, it follows that the resistance conferred by short range obstacles is dynamic; i.e. this resistance will be partly determined by the external deformation variables of temperature and imposed deformation rate.

Long range obstacles are termed *athermal* obstacles because the dislocation-obstacle interaction occurs over too great a distance for thermal activation; thus mobile dislocations must overcome them by the application of stress alone. The resulting release of dislocations is said to be mechanically-activated or time independent. However, time independent release is never admitted except perhaps at at 0 K for which thermal activation is not possible, or at a sufficiently high enough temperature for which short range

obstacles become thermally transparent. Consequently, low temperature deformation is viewed as being *entirely* dynamic, but the flow stress is only partly so.

It is expected that the stress field experienced by a moving dislocation at any point in a crystal will be the algebraic sum of all stresses at that point [7]; i.e. the short range stresses arising from thermal obstacles will simply be superimposed onto the long range stresses arising from athermal obstacles. The simplest assumption is that the flow stress (σ) can be split into two additive parts:

$$\sigma = \sigma_e + \sigma_s, \tag{1.1}$$

where σ_e is the *effective* stress which exactly matches the dynamic resistance conferred by short range obstacles, and σ_s, the residual, is by definition the long-range *static* resistance of the solid. A literal interpretation of Eq. [1.1], if the effective stress is the only rate sensitive component of the strength, is that deformation occurs only when the applied stress is in excess of the static resistance of the material. In principle then, Eq. [1.1] predicts that if, during a strain *vs* stress tensile test for example, the flow stress is reduced abruptly by an amount equal to σ_e, the deformation ceases; i.e. the strain rate goes to zero. To illustrate this point, an experiment of this type was done in the earlier study [3] of IF-iron at room temperture. For a stress rate of 0.2 MPa/s, a stress decrease of 4.6 MPa (the value of the calculated effective stress) reduced the strain rate to zero. The result is remarkable, considering that the static strength for this material not only dominates the strength at large strains because of strain hardening, but also at smaller strains near the yield stress, which is about 70 MPa (0.2% offset). Of course in order to perform such a test, without trial and error, the effective stress must be known *a priori*.

1.2 Rate Equations

The treatment of low-temperature deformation is by the theory of thermally activated flow, in which barriers to elementary units of flow are overcome by applied stress and thermal fluctuations. The units of flow are modelled as dislocation segments which are held up at short–range obstacles, waiting for thermal activation. It is usually true that the average dwell time at an obstacle is much longer than the average transit time between obstacles. Thus, the release rate of dislocation segments from obstacles, which is the reciprocal of the average dwell-time, accounts for the time and temperature dependences of the deformation. The release rate is given by an Arrhenius rate equation, which is the product of an attempt frequency and the probability of a successful thermal fluctuation. The strain rate is then, simply, the release rate times the strain produced by a successful thermal fluctuation. The usual form of the strain rate equation, for a single thermally-activated mechanism, is:

$$\dot{\epsilon} = NAb\nu \exp\left(\frac{-\Delta G}{kT}\right) = \dot{\epsilon}_o \exp\left(\frac{-\Delta G}{kT}\right) \tag{1.2}$$

where N is the number of activation sites per unit volume, A the area swept out by a dislocation segment per thermally-activated event, which is given as the product of the dislocation segment length (l^*) and the distance of motion after activation (d^*), b the Burgers' vector, ν the attempt frequency, ΔG the Gibbs free energy of activation, and $\exp(-\Delta G/kT)$ the probability of a successful thermal fluctuation. Additionally, ΔG is usually expressed as $\Delta G = \Delta H - T\Delta S$, where ΔH is the activation enthalpy, and ΔS the activation entropy, at constant temperature.

Both $\dot{\epsilon}_o$ and ΔG will depend upon stress, temperature and structure, but in the analysis of temperature and strain rate effects on deformation, the dependence of $\dot{\epsilon}_o$ is assumed weak in comparison to that of ΔG. Of particular interest here is the stress dependence of ΔG which mainly controls the strain rate at a particular temperature.

The variation of ΔG with stress is given as

$$\Delta G = \Delta G_o - \int_0^\sigma V^* \, d\sigma \tag{1.3}$$

where $V^* = (\partial \Delta G / \partial \sigma)_T$ has the dimensions of volume and is referred to as the *activation volume*. Within a limited range of stress and temperature, the stress dependence of the activation energy may be linearised. Then, the amount of energy provided by the applied stress (i.e. the work done) is equal to $V^* \sigma_e$. Thus, an increase in the effective stress has the effect of reducing the activation energy and increasing the rate of thermal release of dislocation segments. Following Eq. [1.2], changes in the external deformation variables, namely strain rate and temperature, may effect changes in the activation energy. In particular, separately raising the strain rate or reducing the deformation temperature (but still maintaining the same strain rate) raises the effective stress and reduces the activation energy.

While the ideas discussed above are sufficient to explain the temperature and rate dependence of deformation, experimental evaluation of all the activation parameters is not usually possible. In particular, ΔS is usually assumed *a priori* to be either zero or temperature and stress independent, conditions which Li [8] suggests may not be appropriate. As well, the utility of this method has been limited by at least the following considerations: (1) a general failure of various theoretical models to distinguish between mechanisms [9,10]; and (2) the insufficient treatment of cases in which competing mechanisms operate [11].

Another form of Eq. [1.2] is used in the literature of dislocation dynamics,

$$\dot{\epsilon} = \rho_m b v, \tag{1.4}$$

which follows from the equalities $\rho_m = Nl^*$ and $v = d^* \nu \exp -(\Delta G / kT)$. This is Orowan's equation [12], which gives the deformation rate in terms of the density of

mobile dislocations, ρ_m, and their average velocity, v. Implicit in this formulation is that the stress dependence of v is assumed to be much stronger than the stress variation of ρ_m. Although $\dot{\epsilon}$ has a precise physical description (Eq. [1.2]), when it is calculated from Eq. [1.4], empirical relations are generally used to describe the stress dependence of v and evolution of the ρ_m with increasing stress and strain.

1.3 Direct Measurement of the Dislocation Velocity

One of the principal achievements in the experimental study of the deformation of materials has been the direct measurement of the velocity of individual dislocations as a function of stress. In general, these measurements involve applying a shear stress pulse of known duration, onto a slip plane of an oriented single crystal, and observing the position of dislocations before and after the application of the stress. Such measurements are useful because they potentially separate the effects of structure from the effects of temperature and stress, and provide a basis for calculating the strain rate. Johnston and Gilman [4] were the first to measure by direct observation, in lithium fluoride, the stress dependence of the dislocation velocity. In this seminal work, they found that the dislocation velocity, at low and intermediate stresses, is described by a power law in the applied stress of the form:

$$v = v_o \left(\frac{\sigma}{\tau_o}\right)^n. \tag{1.5}$$

Here, τ_o and n are material and temperature dependent constants. τ_o is the stress required to move a dislocation at unit velocity, v_o; in this paper we take $v_o = 1.0$ m/s. n, the power exponent, is descriptive of the stress sensitivity of the dislocation velocity. In LiF, the dislocation velocity was found to be a very sensitive function of the applied stress, increasing by the the twenty-fifth power.

Johnston and Gilman found that the relation given by Eq. [1.5] was applicable for a

range of velocities that spanned eight orders of magnitude from 10^{-9} m/s, which defined a minimum stress for dislocation motion, to 10^{-1} m/s, at high stress, which is about 4.5 orders of magnitude below the limiting velocity of transverse sound waves in the material. It may be noted here, that while the power law equation has no theoretical basis, it has been shown to give a good representation of the data over the useful range of velocities normally encountered in engineering applications [14]–[30].

Combining the concept of the stress dependence of the dislocation velocity with a determination of the strain dependence of the mobile dislocation density, Johnston and Gilman [4] devised a model to calculate stress *vs* strain curves, in which n was a key parameter. Later, Johnston [13], with the aid of a IBM-704 computer, calculated various mechanical behaviours including stress *vs* strain curves, yield point phenomenon and delay times in creep tests.

The success and novelty of Johnston and Gilman's work, which demonstrated the importance of the concept of the stress dependence of the dislocation velocity, generated much interest in the study of dislocation dynamics and measurements of dislocation mobilities in other materials. However to date, some thirty years later, dislocation velocities have been measured in only a few materials: among the metals are W [14], Mo [15,16], Fe [17], Fe-Si [18], Nb [19], Zn [20], Ni [21], Cu [22,23], Cu-Ni [24,25], Cu-Al [26], Cu-30%Zn [27], Ti [28], Al [29], Pb and Pb-In [30]; some data are also available for a few materials having the diamond, sodium chloride and sphalerite structures. It is true that the use of direct methods to determine the stress dependence of the dislocation velocity is severely limited, particularly by the difficulty in acquiring single crystals, reliable etchants, elaborate and special mechanical devices and then the tedium inherent in making a sufficient number of measurements.

1.4 Indirect Methods of Determining n

As a consequence, there has been interest in establishing techniques which are simpler and more convenient than the direct methods to determine the stress dependence of the dislocation velocity. To this end, Guard [31] suggested that if there is a simple stress-dependent velocity change on change of strain rate according to Orowan's equation, then the stress dependence of the dislocation velocity could be determined indirectly by measuring the logarithmic stress sensitivity of the strain rate, i.e.

$$n^* = \frac{d\ln\dot{\epsilon}}{d\ln\sigma}. \tag{1.6}$$

Here, n^* is usually determined as the reciprocal of the strain rate sensitivity of the flow stress, $n^* = 1/m$, measured by an "instantaneous" crosshead speed change test in the conventional hard machine. (In these tests, the stress change is usually measured in response to an imposed abrupt *upward* change in the crosshead speed.) Accordingly, Guard measured the stress sensitivity in Fe-3.25%Si and observed its value was of the order of 60. This value is much larger than the intrinsic value, $n = 35$, measured by Stein and Low [18] using direct methods.

The reasons for this discrepancy have been extensively discussed in the literature of dislocation dynamics. One possibility is to suppose that not only the velocity but also the mobile dislocation density changes in response to the upward change in crosshead speed. An increase in the mobile density would occur, according to Johnston and Stein [32], if the sudden increase of stress unpins some of the dislocations that have become immobilized in the network by strain hardening. Alternatively, Alden [3] has suggested that sources may operate to increase the total dislocation density. Using the power law equation for the dislocation velocity, the measured stress sensitivity becomes

$$n^* = n + \frac{d\ln\rho_m}{d\ln\sigma} \tag{1.7}$$

where n is the stress sensitivity associated with velocity change alone. Evidently, $n^* = n$ when the increase of stress neither generates many new dislocations nor unpins those previously stuck.

Other analyses [33,34] have emphasized that it is the effective stress, not the total applied stress, which drives the dislocation velocity, and that the effective stress is usually less than the applied stress, Eq. [1.1]. (Note that when measurements of dislocation velocities are done at small strains in single crystals having exceptionally high purity and perfection, the static component of the flow stress can be assumed to be relatively small in comparison to σ_e; i.e. $\sigma_e \approx \sigma$.) This will be true even in the annealed material if it possesses a microstructure that contributes an initial static strength; then the effective stress will be less than the flow stress even at very small strain. As well, at larger strains the static strength will increase because of strain hardening, which is assumed to be mainly or entirely rate insensitive. Thus it can be argued that the dislocation velocity, as defined by Eq. [1.5], must be given as a function of σ_e, rather than σ. The first term of Eq. [1.7] becomes

$$\frac{d\ln v}{d\ln \sigma} = n\frac{d\ln \sigma_e}{d\ln \sigma} \tag{1.8}$$

If the effective stress is the only rate sensitive component of the flow stress, then on change of crosshead speed, $d\sigma_e = d\sigma$. Thus

$$\frac{d\ln v}{d\ln \sigma} = n\frac{\sigma}{\sigma_e} \tag{1.9}$$

and, in most instances, n^* will be larger than n, even at the yield stress (and increasingly so at larger strains). Accordingly, a simple linear extrapolation of the strain rate sensitivity data to zero strain, as suggested by some investigators [32,35], does not give $n^* = n$.

In general, the differences between n^* and n may be attributed to both changes in the mobile density and an effective stress to flow stress ratio less than unity. Unless, however.

we can know the relative importance of these effects, strain rate or stress sensitivity data do not permit a determination of n. The theoretical resolution of these problems is particularly relevant to this thesis, in which stress sensitivity data will be used to determine the dislocation velocity constants, n and τ_o.

1.5 Progress in Modelling n^* Data

Recent progress has been made in the modelling of the strain rate sensitivity of a select group of materials for which a comprehensive set of rate sensitivity data is available. This progress is primarily the result of attempts to model the mobile dislocation density. In a study by Pharr and Nix [34], the total dislocation density is given by a linear function of the strain, following Johnston and Gilman, and the mobile density is determined by the fraction of links of the dislocation network longer than a critical length

$$L_c = \frac{\alpha G b}{\sigma_e}. \tag{1.10}$$

This model was applied with considerable success to Fe-3.25%Si and copper, materials that are both rate insensitive (i.e. large n^*), but show major differences in the evolution of structure and effective stress. However, the predicted values of n^* for iron, the only rate sensitive material they studied, were much larger than the values determined from experiment. This discrepancy resulted largely from the model's apparent over estimation of the stress sensitivity of the mobile dislocation density.

In a parallel study, in which the strain rate sensitivity of iron was studied by application of a model of mobile dislocation density having a different physical basis from Eq. [1.10], Alden [36] was able to make successful predictions of the experimental results. In addition, the model was shown to have good predictive capabilities for other materials, LiF and Fe-3.25%Si. (This model will be described in the following section.)

Alden's model differs from the model of Pharr and Nix [34] in two ways: (1) the total dislocation density is determined by the stress, not the strain; and (2) the mobile dislocation density is determined from a competition, over time and strain, between stress rate (mechanically-activated) dependent generation and velocity dependent trapping.

Despite these theoretical differences, a similar result of both models is that an upward change in the crosshead speed is followed by an abrupt increase in the mobile dislocation density. In Pharr and Nix's model, this increase results because the critial link length decreases in response to a higher effective stress. In Alden's model, new dislocations are injected into the material in response to the high stress rate transient following the crosshead speed change. In light of these studies, it appears that the evaluation of the stress sensitivity of the dislocation velocity by way of an upward change of crosshead speed is complicated by a structural change.

1.6 Equations of the Model

1.6.1 The Mobile Density

The theory has been discussed in two earlier papers [5,38] and its essential equations will only be briefly described here. The basis for the theory is an empirical relation linking the total dislocation density [39,40,41] to the applied stress, namely

$$\sigma = \sigma^* + \alpha G b \rho_t^{1/2}. \tag{1.11}$$

σ^* is an experimental constant which is attributed to sources of hardness other than dislocations. In the theory, σ^* is a *frictional* stress which defines the threshold stress at which moving dislocations begin to multiply. Following the observations of Johnston and Gilman, we take σ^* to be the stress required to move dislocations at the velocity of $10^{-9} m/s$.

Time independence is implied by Eq. [1.11]; i.e. the total dislocation density depends on the level of stress, not the rate of stress increase. Thus, we assume that dislocation sources, which generate additional dislocations, are activated mechanically by the monotonic increase of stress. Consequently, in taking the time derivative of Eq. [1.11] and making the assumption that all newly generated dislocations are mobile, we obtain the result that the generation rate is linked to the rising stress;

$$\dot{\rho}_m^+ = \frac{2\rho_t^{1/2}}{\alpha G b}\dot{\sigma}. \tag{1.12}$$

Once dislocations are generated, they move at a characteristic velocity v to produce strain. After moving over a distance r_o, the mean free path, they are trapped (i.e. immobilized) in the dislocation network. The attrition rate for the mobile population is

$$\dot{\rho}_m^- = -\frac{\rho_m}{t^*}, \tag{1.13}$$

where $t^* = r_o/v$ is the statistical lifetime. Thus, the net change in the mobile density is a consequence of a competition between stress rate dependent generation and velocity-dependent trapping,

$$\begin{aligned} \dot{\rho}_m &= \dot{\rho}_m^+ + \dot{\rho}_m^- \\ \dot{\rho}_m &= \frac{2\rho_t^{1/2}}{\alpha G b}\dot{\sigma} - \frac{\rho_m v}{r_o}. \end{aligned} \tag{1.14}$$

1.6.2 The Dislocation Velocity

The dislocation velocity is given by a power law in the effective stress:

$$v = v_o \left(\frac{\sigma_e}{\tau_o}\right)^n. \tag{1.15}$$

τ_o is a constant descriptive of the frictional resistance to dislocation glide, and is defined as the stress required to move a dislocation at a velocity of $v_o = 1\ m/s$. σ_e is given by:

$$\sigma_e = \sigma - \alpha G b \rho_n^{1/2}, \tag{1.16}$$

which contains the assumption that network dislocations contribute to strain hardening by raising the static strength of the material. In a recrystallized material, an initial network dislocation density is assumed in order to account for the contribution to the initial static strength made by residual dislocations.

1.6.3 Strain Hardening

The strain hardening coefficient is defined as the derivative of the static strength with respect to strain:

$$\theta = \frac{d\tau_s}{d\epsilon} = \frac{\alpha G b \dot{\rho}_n^+}{2\dot{\epsilon}\rho_n^{1/2}}. \tag{1.17}$$

This equation can be rewritten recognizing that the rate of increase of the network dislocation density $\dot{\rho}_n^+$ is exactly equal to the attrition rate of the mobile dislocation population $-\dot{\rho}_m^- = \rho_m \nu / r_o$:

$$\theta = \frac{\alpha^2 G^2 b}{2 r_o \tau_s}. \tag{1.18}$$

If the trapping mechanism is the formation of an attractive junction with a second, intersecting dislocation (which may be either mobile or already trapped in the network), then the mean free path should vary with the mean dislocation spacing ($\rho_t^{-1/2}$), factored by some statistical likelihood that such an encounter will form a stable attractive junction. Thus we write $r_o = T^*/\rho_t^{1/2}$, where T^* is the statistical constant. The mean free path falls in proportion to $\rho_t^{1/2}$ as a result of the refinement of the dislocation network through dislocation trapping. This leads to linear hardening. However, it is known from experiment [39] that iron does not harden linearly. Instead, like other body-centered cubic metals, iron exhibits parabolic hardening. This result implies that a constant mean free path determines the strain hardening coefficient. (It is not known whether some other feature of the microstructure controls the strain hardening rate, such as large athermal precipitates or cell walls, or some competitive softening process, e.g. dynamic recovery.

which lowers the strain hardening rate by releasing network dislocations.) Despite this uncertainity, the mean free path is estimated by fitting the slope of the strain *vs* stress curve at intermediate strain.

1.7 Applications of the Model

There is a growing body of literature suggesting that this theory is both accurate and useful. In particular, quantitative predictions have been made of (1) the strain rate sensitivity of the flow stress of LiF, Fe-3.25creep in 304 stainless steel [5], (3) yield stresses of a wide variety of materials [37], and (4) more recently the dynamic properties of iron at room temperature.

Among the various applications, the determination of the constants of the velocity equation, n and τ_o, is our primary effort, since these material constants control the dynamic properties of dislocations. In this present study, these constants are derived from a theoretical fit to experimental measurements of the stress sensitivity of the strain rate (Eq. [1.6]).

1.8 Stress Decrease Experiments in the Soft Tensile Machine

The usual method used to obtain stress sensitivity values is to measure the change of flow stress in response to an "instantaneous" crosshead speed change in a conventional hard machine. However, this method can be severely limited if the material is rate insensitive, which happens either because n is large, as it is for Fe-3.25%Si, or τ_o is small as for copper. In this case, a large change in the strain rate is accompanied by a small change in the flow stress, which may not be accurately measured. On the other hand, a material that is rate insensitive is, by definition, stress sensitive. Thus, a small change in the applied stress will produce a large change in the strain rate. Therefore, a better

method of measurement is to apply this small stress change. Such an experiment can easily be done in the soft tensile machine, in which the stress and rate of stress increase are controlled and the extension and extension rate are measured.

We choose to employ a stress drop because the theory (Eq. [1.11]) indicates that an increase of stress will result in a burst of dislocation generation. However, if a stress drop is imposed, the mobile density is unchanged in the instant of the stress drop, and afterwards, only slowly declines with time and strain. (Later, it begins to increase again; see below Section 3.5.1). Consequently, the measurement of the stress sensitivity will not be complicated by a structure change. Instead, the decrease in strain rate will be proportional to the decrease in the dislocation velocity; i.e.

$$n^* = \frac{d\ln\dot{\epsilon}}{d\ln\sigma} = \frac{d\ln v}{d\ln\sigma}, \tag{1.19}$$

and from Eq. [1.9]

$$n^* = n\frac{\sigma}{\sigma_e}. \tag{1.20}$$

Chapter 2

Experimental Methods

2.1 Sample Preparation

The test metal is IF iron, supplied by ARMCO, of composition shown in Table 2.1. This is a pure iron doped with titanium to remove residual interstitial carbon and nitrogen; it is nominally interstitial free. Slender tensile specimens are stamped from sheet having an as-received thickness of 0.09 cm. These specimens have a parallel gauge length of about 2.54 cm with a typical cross-sectional area of 2.25 mm^2. Prior to annealing, specimen surfaces are given a 600 grit polish, followed by a brief ultrasonic agitation in ethanol. Annealing is done in high vacuum at 820 °C for 64 h. The recrystallized grain size, as a mean linear intercept, is 15 μm. Some supplimentary specimens were also prepared from cold rolled sheet, having a reduced thickness of 0.06 cm; after recrystallization, the grain size in these specimens was 35 μm. Prior to testing, specimens are chemically polished for 10 to 20 s in a 3 % hydrofluoric acid, hydrogen peroxide solution.

Table 2.1: Composition of ARMCO IF-iron.

C	Mn	N	Ti	Nb	P	S	Si	Al
0.004	0.31	0.018	0.056	0.071	0.008	0.022	0.011	0.036

2.2 Stress Drop Tests

Tests are performed in a soft tensile machine of the Andrade-Chalmers (cam) type in which the rate of increase of stress is controlled and the specimen extension is measured. The load is applied by dead weight through a lever of a variable moment arm (Figure 2.1(a)). The arm is designed such that, for any instantaneous load P and independent of changes in specimen length, the stress σ is given by the equation $\sigma = 4P/A_o$; A_o is the initial specimen area. Various stress rates are achieved by varying the density and flow rate of particulate matter into the loading container. In these tests, stress rates ranging from 6.5×10^{-3} to 5.0 MPa/s are achieved by using lead shot and glass balls, sized for 2 mm diameters, and two fractions of Ottawa sand (ASTM C109), screened for -35 to +50 mesh and -50 mesh. The time and rate of flow of lead shot and glass balls are controlled by a motor driven shutter of variable diaphragm. Delivery of sand is through pyrex funnels which are flamed to produce different openings.

Specimen extension in the stress drop tests is measured by a clip-on extensometer MTS model 632.27C-21 of gauge length one inch (2.5 cm), calibrated 0 to 10 V for 0.02 inch extension (0.051 cm). (Another extensometer, MTS model 632.11C-21 calibrated for 0.15 inch extension (0.38 cm), is used to determine strain *vs* stress curves.) A Honeywell Accudata 218 bridge-amplifier also provides a low-pass filter of 100 Hz. The output signal is digitized using a sampling interval which is scaled to be appropriate to the stress rate of each test. The digital recording instrument is a Bascom Turner model 5120, which writes sequential files of extensometer voltage to floppy disc. These data may be either retrieved and analyzed using the built–in functions provided by the Bascom Turner or transferred to a microcomputer. In most tests, because the loading times are long, only a portion of the loading *vs* time curve that pertains to the stress decrease is recorded by the Bascom Turner; about 5 MPa of loading is recorded prior to

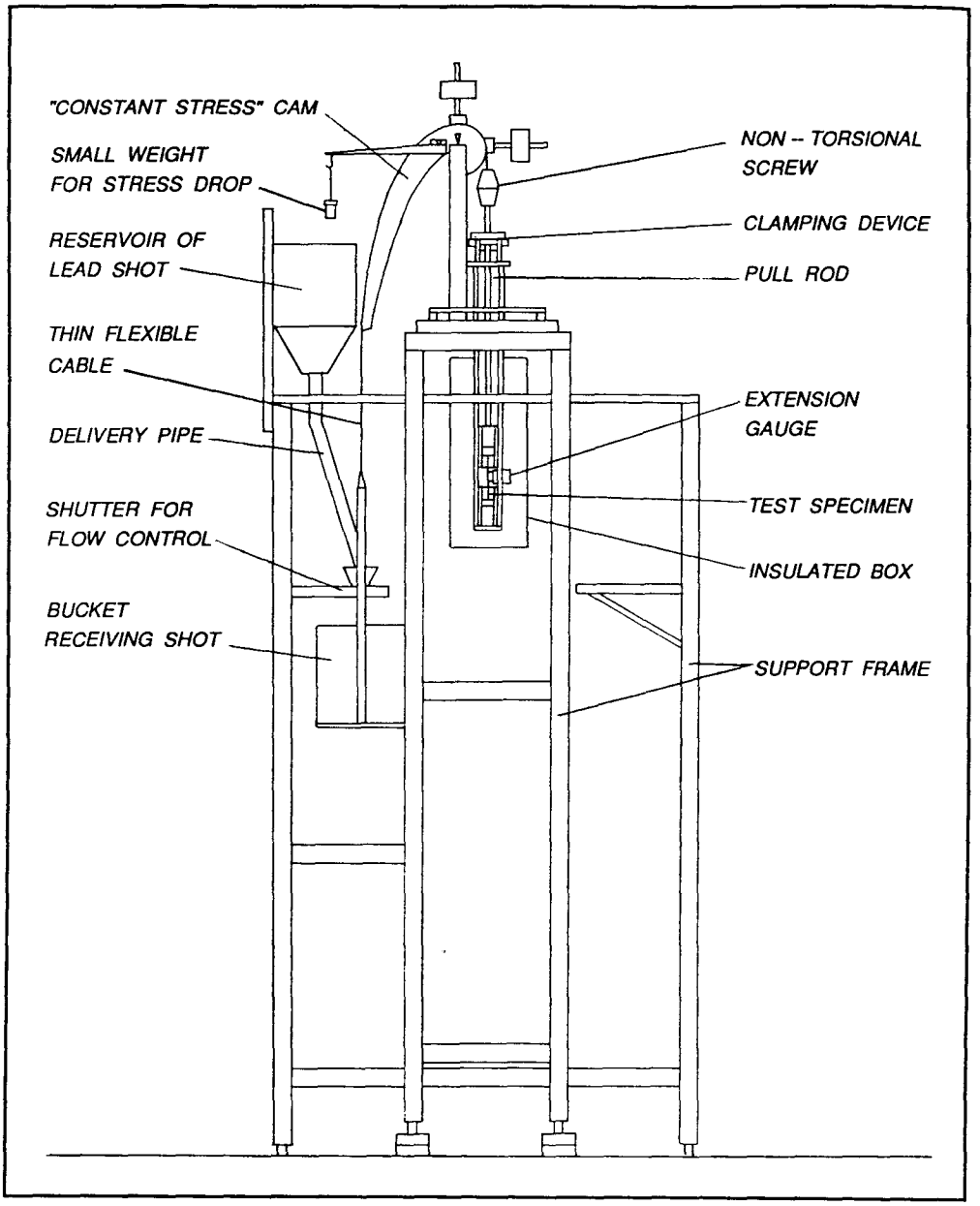

Figure 2.1: Schematic diagram showing the essential features of a soft tensile machine.

the stress drop and another 5 MPa afterwards. In total 2000 data points are acquired. In addition, specimen extension *vs* time is charted continuously with a Honeywell E196 chart recorder.

For low temperature testing, a steady stream of cooled nitrogen gas is admitted into an insulated box constructed from 5 cm thick polystyrene foam. The stream of nitrogen gas is adjusted by a valve; in this way, temperature control better than ± 0.5 °C is routinely achieved. Test temperature is measured with a copper-constantin thermocouple attached to the lower grip and monitored by a Fluke 8502A digital multimeter.

A typical stress drop experiment involves several tests on a single specimen at constant stress rate but increasing stress. A "safe" prestress intended to be below the elastic limit is applied at the start of each test. After about 1.0 % inelastic strain, while the stress continues to rise, a small stress decrease is imposed by lifting a small weight, which hangs from a lever attached to the cam, and was a small addition to the total weight supported by the specimen. The specimen extension rate is measured both before and after the stress drop. At the start of each test, the output voltage of the extensometer is zeroed by repositioning its knife edges on the specimen to re-establish the one inch initial gauge length. For the low temperature experiments, the thermocouple voltage is monitored continuously and the flow of cooled nitrogen gas adjusted to insure that testing proceeds at the targeted temperature. Initial cooling takes approximately 1 h compared to about 15 min between consecutive tests. Once thermal equilibrium has been established, the temperature is fairly stable and requires only slight adjustment.

2.3 Stress versus Strain Tests

Stress *vs* strain tests are performed in a conventional Instron machine, in which the rate of specimen extension is controlled and the load is measured. In these tests, careful

consideration has been given to the rigidity and alignment of the testing system. To avoid sloppy linkages, pins and universal joints have not been used; instead the pull rod is screwed directly into the load cell and is held firmly in place by a wide-faced nut. Specimen grip sections are bolted against file inserts. The lower grip is bolted to the lower cage and the upper grip is held firmly by a nut on the threaded pull rod. Alignment of the grip faces is achieved by shimming the load cell at three points. Good alignment is determined visually. Easy mounting, to ensure the vertical alignment of the specimens, is achieved by mounts slotted to exactly accommodate the width of the specimen grip sections (about 4.8 mm). Near axial loading of the specimen is insured by offsetting the file inserts of the grips by half of the specimen thickness.

Specimen load is measured using a FR load cell calibrated 0 to 10 mV for 200 lbs (890 N). The output signal from the load cell amplifier is digitized using a sampling interval which is appropriate to the crosshead speed of the test. In most tests, 10 000 points are stored for 0.34 cm extension. An external low-pass filter of 10 Hz filters high frequency noise. The cut-off frequency is sufficiently high to filter the output signal without loss of detail of the inelastic transient at yielding for the highest crosshead speed tests. The digital recording instrument is a Bascom Turner model 5120. Load *vs* time is also monitored continuously on chart. At the start of each test, both the Bascom Turner and chart recorder are zeroed on a sensitive (20 pound) load scale, while the specimen is fixed in the top grip but not yet attached to the lower grip.

For low temperature testing, very accurate temperature control is necessary, as the loads developed in the rigid system are particularly sensitive to temperature variation. In these tests, cooling is provided by chilled alcohol with magnetic stirring. The container is a foam insulated, 4000 L pyrex beaker. Fine temperature adjustment is made by admitting small amounts of liquid nitrogen, from a pressurized liquid nitrogen dewer, through the inlet of a small diameter copper tube immersed about 5 cm below the surface

of the alcohol. Temperature control of this apparatus is within ±0.2 °C. Load cycling was used to avoid overstressing specimens during initial cooling.

Specimen extension is determined from the difference between the total crosshead displacement and all elastic deflections of the "machine" (these include all other deflections, besides the elastic and inelastic elongations of specimen gauge length, such as the crosshead, grips, linkages, load cell, and specimen shoulders). The total extension of the specimen gauge length at a particular time t is

$$\Delta l_t = \dot{X}t - \frac{P}{K}, \tag{2.21}$$

where $\dot{X}$ is the crosshead speed, P the specimen load and K the machine stiffness, which is the composite spring constant of the elastic elements of the machine. K is determined to be 7.5 MN/m by an elastic loading method using a strain hardened specimen (see Appendix A.2). K is assumed to be constant throughout the tests.

The use of Eq. [2.21], by definition, confines all inelastic deflections to the specimen gauge length including deformation that may occur outside the reduced (parallel) section, particularly in the fillets of a tensile specimen. This necessitates that the initial gauge length l_o be treated as an operational length, over which the shoulder–to–shoulder extension is distributed to give a strain equal to the strain measured within the parallel section [44]. Accordingly, l_o = 2.86 cm is determined from a separate calibration (see Appendix A.1).

2.4 Model Simulations

The time integration of the equations of the model (Eq's [1.11-1.18]) permits the calculation of all the mechanical and microstructural quantities as they develop during the deformation testing of IF iron. Among the principal mechanical quantities calculated are stress, strain, strain rate, slope of the strain *vs* stress curve and strain hardening

Table 2.2: Material constants used in the theoretical calculations

Temperature (K)	n	τ_o (Pa)	r_o (m)	α	G (Pa)	E (Pa)	b (m)
298	2.0	3.6×10^{9}	4.5×10^{-6}	0.33	7.18×10^{10}	2.11×10^{11}	2.48×10^{-10}
273		*to be determined*		"	7.27×10^{10}	"	"
253		*to be determined*		"	7.32×10^{10}	"	"
198		*to be determined*		"	7.36×10^{10}	"	"

coefficient. Also calculated are the microstructural quantities including the generation rate of mobile dislocations, rate of trapping in the network, mobile density, network density, dislocation velocity and mean lifetime. The integration is done numerically by an iterative procedure using a 486-33 MHz microcomputer. The time interval of integration Δt depends on the stress rate (or crosshead speed). For convenience, the interval chosen is the time to achieve a stress increase of about 0.01 MPa in one iteration. This interval insures that the maximum loss of the mobile dislocation content to the network in any one iteration is less than 1.0 % of the mobile density, i.e. $\Delta t/t^* < 0.01$.

The initial values of some of the principal variables are (1) strain and stress = 0, (2) network dislocation density $\rho_n = 10^9$ m^{-2} and mobile dislocation density $\rho_m = 10$ m^{-2}, and (3) velocity $v = 0$ up to the elastic limit stress, then by definition, $v = 10^{-9}$ m/s. All these quantities increase with further increases of stress. The choice of the initial dislocation network density reflects a typical low residual content of an annealed metal. Since it is likely that most of these residual dislocations will be immobile (either they are severely pinned or do not lie on a glide plane), ρ_m will be practically zero. However, assigning to ρ_m a particular low value is not a critical decision since ρ_m will increase very rapidly once dislocation generation begins. However, setting $\rho_m = 0$ causes a division–by–zero–error for some of the calculations.

The material constants that have been employed in the calculations are listed in Table 2.2. Note that n, τ_o and r_o at the lower temperatures are yet to be determined from

experiment and model calculations. The model material is a single crystal in comparison with the polycrystalline experimental material, and calculations are of shear stress and shear strain; the factor 2.75 is used for conversion to tensile stress and 1/2.75 for tensile strain. The Burgers vector $b = 2.48 \times 10^{-10}$ m. For each temperature, the value of the shear modulus G is calculated in the direction of slip and on the slip plane, according to the analyses given for cubic metals [42];

$$\begin{aligned} G &= C_{44} - \frac{1}{3}H \\ H &= 2C_{44} + C_{12} - C_{11}, \end{aligned} \tag{2.22}$$

where the C_{ij} values are the appropriate temperature dependent elastic constants for iron [43]. The Young's modulus listed is the polycrystalline modulus at ambient temperature (its precise value is not important).

Simulations have been done for four distinctive kinds of deformation tests. At constant stress rate the model generates (1) soft machine tensile curves of strain *vs* stress. If at some point the stress is reduced by a small amount, then the material continues to deform but at a slower rate under a lower effective stress. For different stress rates and stress decreases, the model calculates (2) the strain rate ratio, and (3) the recovery time of the strain rate to its prior maximum value. At constant crosshead speed, the model generates (4) conventional hard machine tensile curves of stress *vs* strain. (The results of crosshead speed change tests or load relaxation tests can also be calculated but have not been done in the present work.) The model accounts for the microstructural differences for tests done at different crosshead speeds so that stress differences between curves can be compared, at the same strain.

In the soft machine simulations, the stress rises steadily at a specified constant rate. In a stress drop experiment, a stress decrease is imposed by a conditional statement at a specified strain of 1.0 %. The strain rate ratio is calculated using the strain rates

developed just prior to, and just after the stress decrease. After the stress decrease, the generation rate of mobile dislocations is set to zero, i.e. $\dot{\rho}_m^+ = 0$, and remains zero until such time as the magnitude of the stress is restored to its prior maximum value; then, generation resumes according to Eq. [1.12].

The hard machine simulation is identical except that the stress rate is derived from the crosshead speed, as well as from the elastic constants of the machine and specimen and the inelastic deformation rate. Consequently, the stress rate is not constant but tends to be high at the start of the stress *vs* strain test, and subsequently decreases with further strain. The analysis of *Holbrook et al* [44] is used to calculate the stress rate;

$$\dot{\sigma} = C\left[\frac{\dot{X}}{l_o g} - \dot{\epsilon}_i\left(1 - \frac{\sigma}{M}\right)\right], \tag{2.23}$$

where $\dot{X}$ is the crosshead speed, l_o is the initial operational gauge length, C the combined specimen–machine modulus, M the effective machine modulus, $g = 1 + e_t$ a variable stretch ratio, and $\dot{\epsilon}_i$ the inelastic strain rate.

Chapter 3

Results and Discussion

3.1 Strain versus Stress

Strain *vs* stress curves were obtained in the soft tensile machine for four temperatures, 25, -20, -50 and -75 °C, and a stress rate of 1.0 MPa/s. These curves (Figure 3.2(a)) show strain, which is the dependent variable in a soft tensile machine test, plotted on the ordinate versus stress, the independent variable, on the abscissa. The stress has been normalized with respect to the shear modulus at 25 °C so that the temperature dependence of the deformation resistance is more usefully shown; i.e. $\hat{\sigma} = \sigma \times G_{298}/G_T$. Inelastic yielding is identified by a rapid initial rise in strain rate[1] (Figure 3.2(b)) to values ranging from about 2.0×10^{-4} s^{-1} at 25 °C to 4.5×10^{-4} s^{-1} at -75 °C. This strain rate increase appears to be the soft machine equivalent of the yield point, seen in a hard machine. In this pure iron, it is quite weak. (At this stress rate, the calculated elastic strain rate is 4.74×10^{-6} s^{-1} and is barely detectable.) The 0.2 % offset yield stress (normalized) is very sensitive to the deformation temperature, increasing from about 81 MPa at 20 °C to 214 MPa at -75 °C.

Strain hardening is shown by the inverse slope of these curves, $1/S = d\sigma/d\epsilon$. It appears to be generally weaker than that described by a parabolic law.[2] That is, S is

[1] Figure 3.2(b) shows the slope $S = d\epsilon/d\sigma$ of the strain *vs* stress curve; the equation for the strain rate is $\dot{\epsilon} = S\dot{\sigma}$.

[2] The usual relation describing strain hardening of body-centred cubic materials is a parabolic curve of the form:

$$\tau = k\epsilon^{\frac{1}{2}}. \tag{3.24}$$

This gives rise to a slope of a strain *vs* stress curve which is not independent of stress, as is characteristic

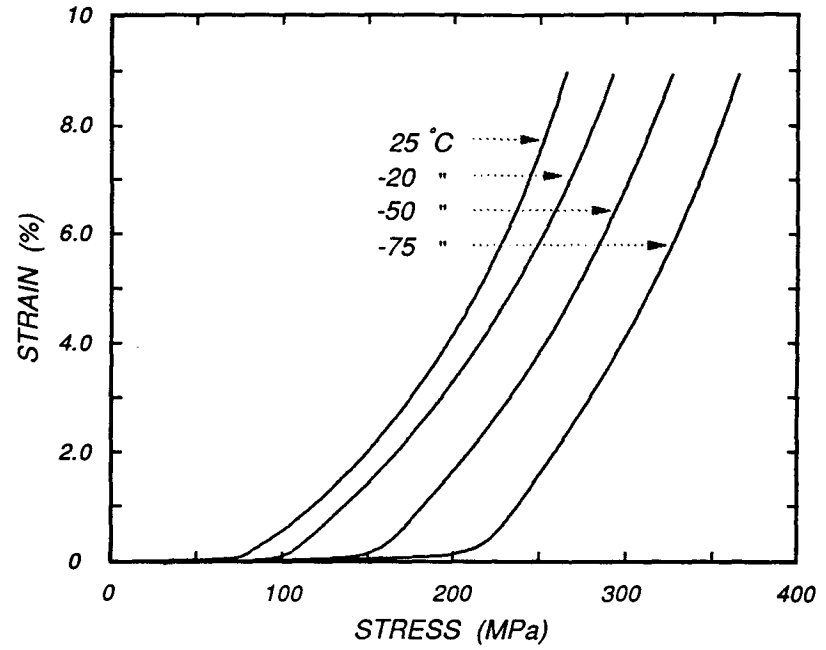

(a)

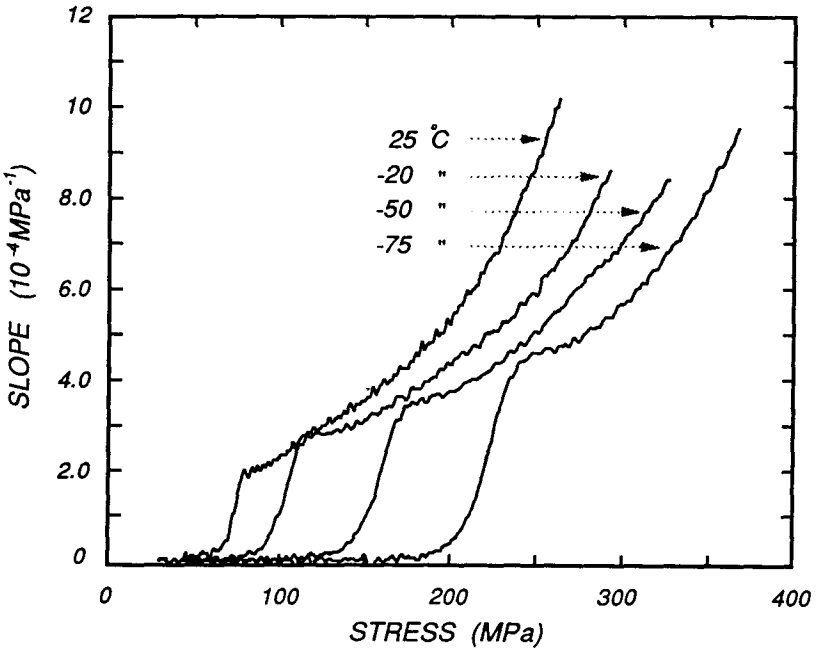

(b)

Figure 3.2: Soft tensile machine (a) strain *vs* stress, and (b) the slope ($\dot{\epsilon}/\dot{\sigma}$) *vs* stress curves at four temperatures, and a constant stress rate of 1.0 MPa/s. The curves have been normalized with respect to the 25 °C shear modulus so that the temperature dependence of the deformation resistance is more usefully shown; i.e. $\hat{\sigma} = \sigma \times G_{298}/G_T$ and $\hat{S} = S \times G_T/G_{298}$.

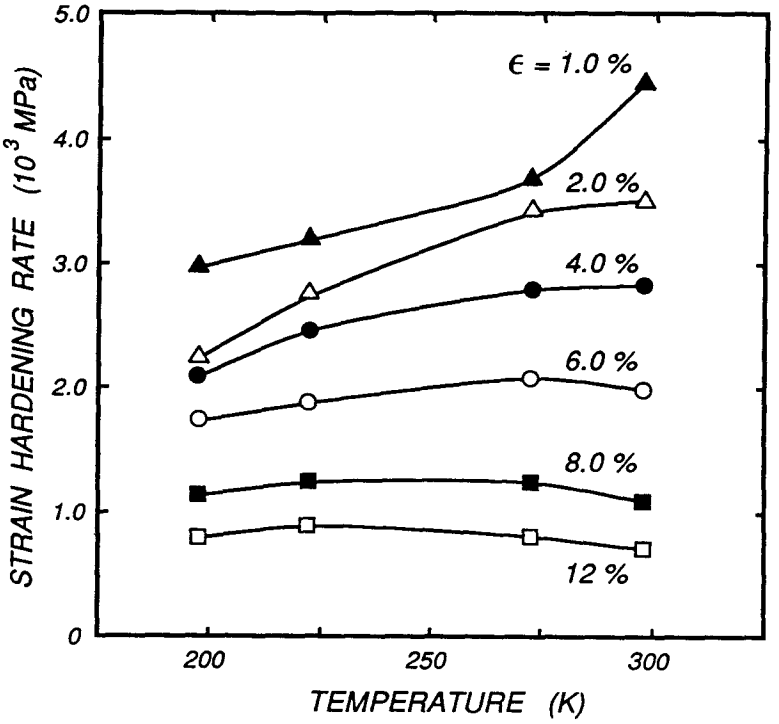

Figure 3.3: Temperature dependence of the strain hardening rate. The curves have been normalized with respect to the 25 °C shear modulus; i.e. $1/\hat{S} = 1/S \times G_{298}/G_T$.

not linear in the stress but rises ever more rapidly as the stress and strain increase. For example, at -75 °C and a stress of 250 MPa, the change of slope with stress ($dS/d\sigma$) is 1.2×10^{-6} MPa^{-2}. At 300 MPa, this change of slope is 3.7×10^{-6} MPa^{-2} and at 350 MPa, 7.0×10^{-6} MPa^{-2} (Figure 3.2).

As well, the strain hardening appears to be sensitive to the deformation temperature, particularly for strains up to about 8.0 % (Figure 3.3). Below this level of strain, the strain hardening rate ($1/S = d\sigma/d\epsilon$) decreases with decreasing temperature. Above about 8.0 % strain, the strain hardening rate is roughly constant. A similar observation of the temperature dependence of the strain hardening rate for iron was reported by Keh [39], who additionally reported that the strain hardening rate approached a minimum at about -75 °C and a maximum value at about 25 °C. (Curiously, Keh observed that the strain hardening rate rises upon further decrease of temperature, below -75 °C.) As a result of the observed temperature dependence of strain hardening rate, the separation between strain *vs* stress curves, at constant strain (Figure 3.2(a)), decreases with increasing strain.

3.2 Stress Sensitivity Measurements

The principal data, from which n and τ_o are determined, are measurements of the sensitivity of the strain rate to a small, abrupt decrease in the applied stress. A typical result is shown in Figure 3.4, which contains the segment of the original experimental digital recording of the extensometer output voltage pertaining to the stress drop; the digital recorder presents pseudo-analog plots of the extensometer output voltage and its time derivative. The smooth line shows extension and the noisy line, the time derivative

of linear hardening, but proportional to the stress;

$$M^2 S = \frac{2}{k^2}\tau. \tag{3.25}$$

calculated by the digital recorder, shows extension rate. In the instant of the stress drop, the extension-time curve falls abrubtly by an amount comparable to the expected elastic contraction of the specimen, and the slope also falls abruptly to an approximately constant value. At later times, and not shown, the slope (extension rate) recovers to its prior maximum value and above; in most of these tests, this happens only after the specimen has suffered appreciable additional strain.

The noise of the time derivative curves is considerable, and seems to increase with the density and flow rate of particulate matter, i.e. with the stress rate. In addition, in prior experience with creep testing using the identical equipment, we have observed that the loading curves are somewhat noisier than creep curves. These effects suggest that at least part of the noise maybe attributed to small variations in the flow of particulate matter, this will likely result in minor differences in inertial loading, and will cause the machine to ring. As well, ringing may result from the initial impact of the flow of shot (in a high loading rate test) onto the bottom of the loading container, and may not be damped-out in the duration of a short test. Another contributing factor to the noise is the high resolution of the extensometer which is not less than about 10^{-5} strain or 2.5×10^{-4} mm. The extrapolated lines in Figure 3.4 show attempts to smooth these data by linear regression, a task which is easily performed by using the analytical functions provided by the digital recorder.

The response of the strain rate to the abrupt stress decrease is measured by the ratio R of the strain rate $\dot{\epsilon}_1$ just before the stress decrease to the strain rate $\dot{\epsilon}_2$ just after; thus $R = \dot{\epsilon}_1/\dot{\epsilon}_2$ will always be greater than unity. The logarithmic stress sensitivity of the strain rate is given by

$$n^* = \frac{d\ln\dot{\epsilon}}{d\ln\sigma} \simeq \frac{\ln R}{\Delta\sigma/\sigma}. \tag{3.26}$$

In this test, the strain rate ratio and the extension rate ratio are identical because the

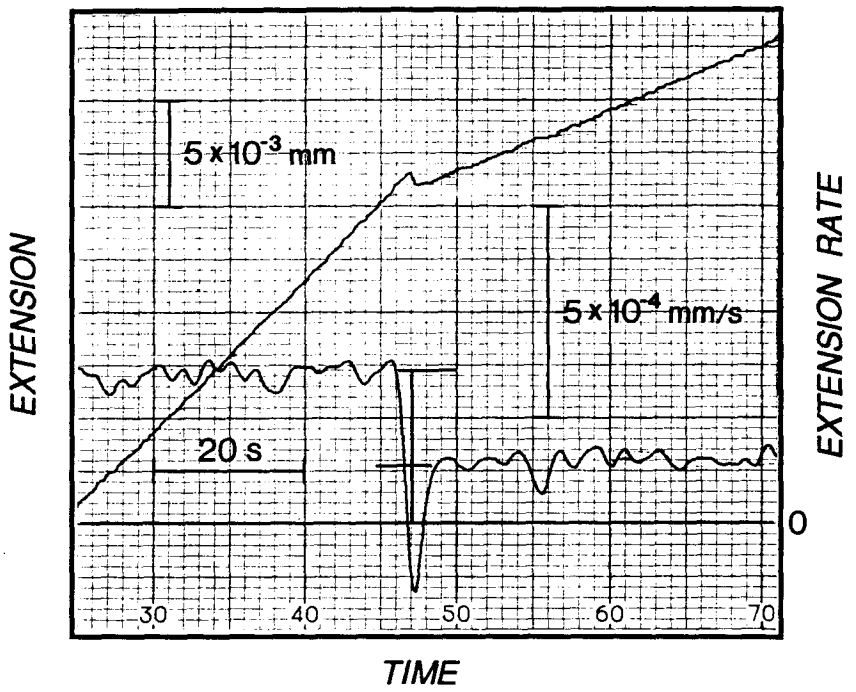

Figure 3.4: The original experimental extension and extension rate *vs* time curves from a typical stress decrease test. The temperature is -50 °C, the stress 305 MPa, the stress rate 0.022 MPa/s, and the stress drop 7.5 MPa. The estimated strain rate ratio is 2.54.

specimen length is unchanged in the instant of the stress decrease, thus $R = \dot{l}_1/\dot{l}_2$. The the extension rates, $\dot{l}_1$ and $\dot{l}_2$, just before and just after the stress decrease are measured by short linear extrapolations of the derivative curves to the time at which the stress is reduced. This point is taken to be the time of the final recorded extension just prior to the stress drop, which is indicated by the peak in the extension *vs* time curve. In this particular test (Figure 3.4), the measured extension rate just before the stress is lowered is 3.625×10^{-7} m/s and just after, 1.375×10^{-7} m/s. The strain rate ratio is 2.54 and the logarithmic stress sensitivity is 39.5.

3.2.1 Effect of Stress and Strain

For a given stress drop, the strain rate ratio is found to be independent of stress and strain at a particular stress rate and temperature. This result seems to be general for low temperature stress sensitivity measurements performed in the soft tensile machine [3,45]. Thus, an average of several measurements on a single specimen at increasing stress and strain can be expected to give a good estimate of the strain rate ratio. A typical result is shown in Figure 3.5(a). Here, the temperature is -75 °C, the stress rate 0.021 MPa/s, and the stress drop 11.5 MPa. The values of the strain rate ratio are scattered about the mean value of 2.56. The estimated standard deviation is 0.064. From Eq. [3.27], it is evident that a constant strain rate ratio arises from an effective stress and velocity exponent which are independent of stress and strain. The constancy of the effective stress is an important result with which to test the theory.

The constancy of the strain rate ratio contrasts with the variability of the stress sensitivity n^*, which rises proportionately with increasing stress (Figure 3.5(b)). According to the analysis of the measured stress sensitivity (Eq. [1.20]), n^* will be linear in the stress if n/σ_e is constant, independent of stress and strain. The slope of the line is 0.089 MPa^{-1}.

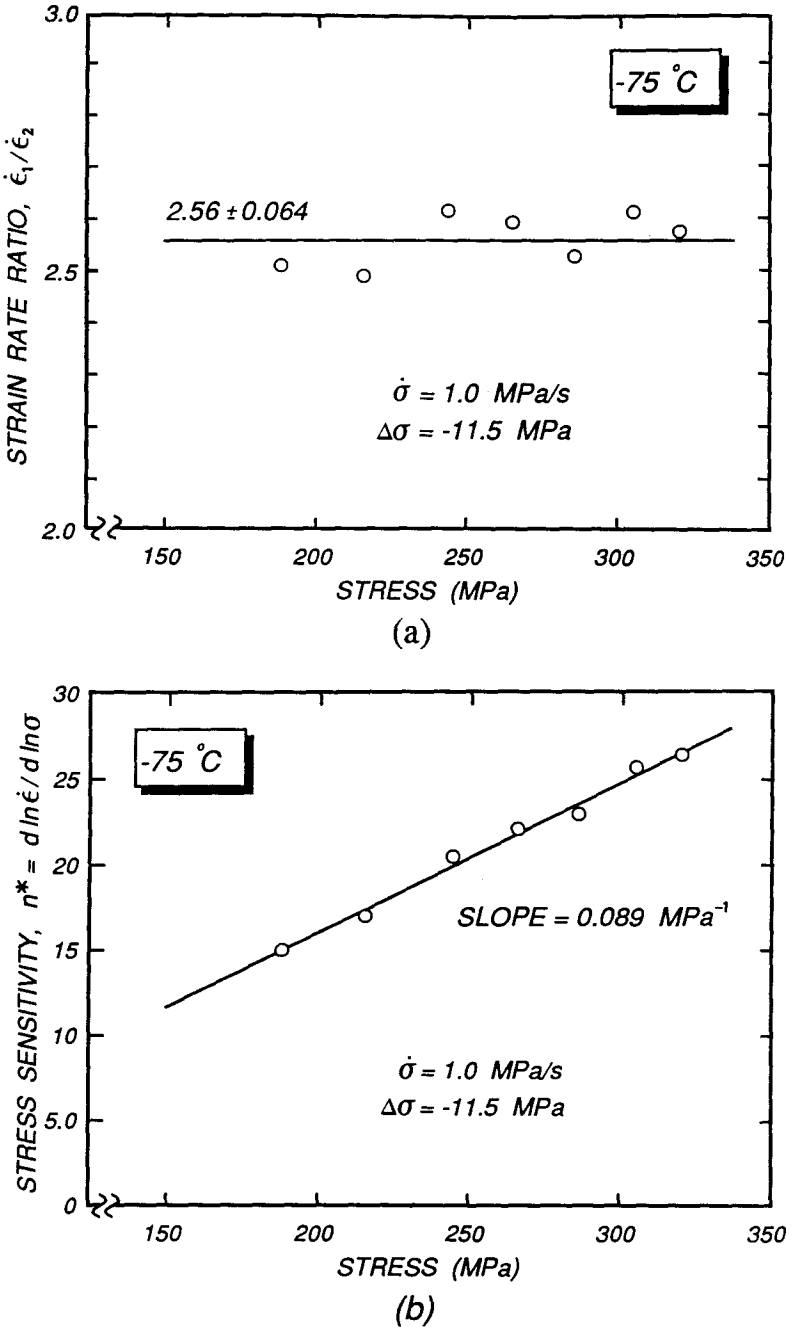

Figure 3.5: Stress dependence of (a) the strain rate ratio, and (b) the stress sensitivity. The temperature is -75 °C, the stress rate 0.021 MPa/s, the stress drop 11.5 MPa, and the estimated strain rate ratio 2.56 ±0.064. The constancy of the strain rate ratio with stress suggests that the effective stress is constant in this experiment.

Extrapolation of the stress sensitivity line back to the value at zero strain has been suggested by some [32,35] to give the velocity exponent n. However, it has been shown [3] that the extrapolated value of n^* and the actual value of n are in gross disagreement for IF iron at 25 °C. This discrepancy is attributed to a flow stress which is larger than the effective stress, even at yield.

3.2.2 Effect of the Magnitude of the Stress Drop

For a given deformation temperature and stress rate (which give a particular value of the effective stress), the strain rate ratio should be approximately exponential in the stress drop; namely,

$$R \simeq \exp\left(\frac{n\Delta\sigma}{\sigma_e}\right), \tag{3.27}$$

as seen by equating Eq's. [1.20] and [3.26]. Experimentally, this relation has been confirmed previously for IF iron at 25 °C [3]. Model calculations will show that Eq. [3.27] is a good approximation if $\Delta\sigma$ is small relative to σ_e, which is usually the case when the value of R is small, i.e. $R \leq 3.0$. Otherwise, R is given by the following exact equation[3]:

$$R = \left[1 - \frac{\Delta\sigma}{\sigma_e}\right]^{-n}. \tag{3.28}$$

Although in this present study, the number of variable stress drop data points obtained for a particular stress rate and temperature are few, the data do appear to be consistent with Eq. [3.27] (Figure 3.6). In this figure, lines have been fitted through experimental points representing three values of stress drop, but for a fixed temperature and stress rate. A forth point is gained for a zero stress drop for which the strain rate ratio is equal to unity, by definition. A single filled point indicates the average of six to seven tests.

[3]This expression can be derived by considering the appropriate strain rate equations: (1) $\dot{\epsilon}_1 = \rho_m b(\sigma_e/\tau_o)^n$ just before the stress decrease, and (2) $\dot{\epsilon}_2 = \rho_m b[(\sigma_e - \Delta\sigma)/\tau_o]^n$ just after the stress decrease; $R = \dot{\epsilon}_1/\dot{\epsilon}_2$. For the case in which $\Delta\sigma$ is small relative to σ_e, the term $1-\Delta\sigma/\sigma_e \simeq \exp(-\Delta\sigma/\sigma_e)$ and Eq. [3.27] holds. This approximation becomes evident when $\exp(\Delta\sigma/\sigma_e)$ is expressed as a series expansion.

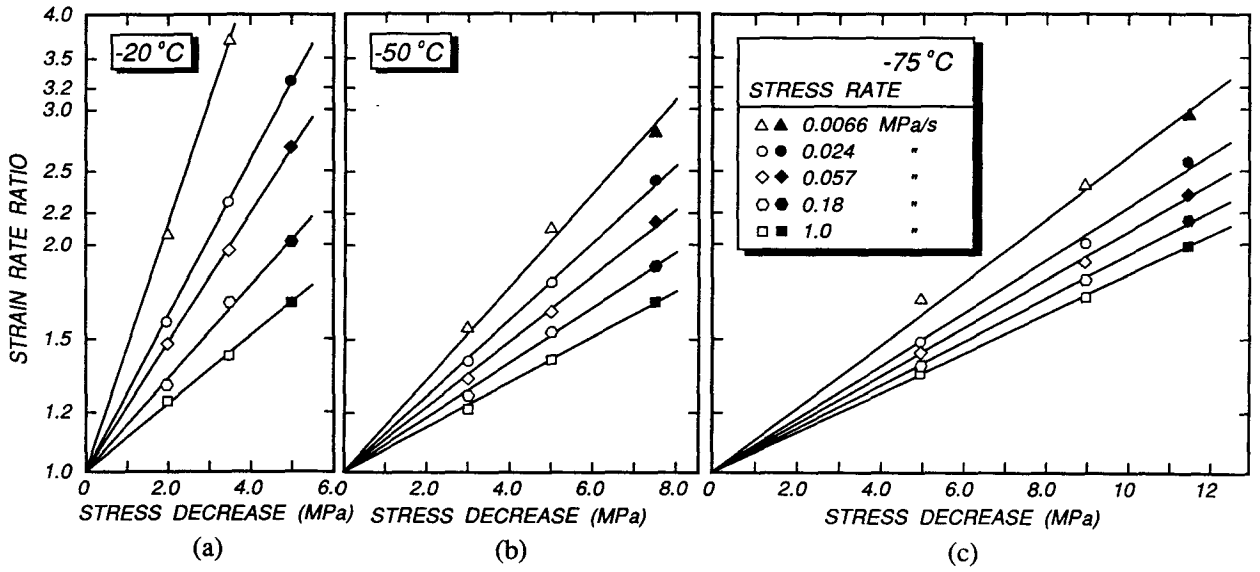

Figure 3.6: Strain rate ratio *vs* stress decrease at several stress rates and three temperatures; (a) -20 °C, (b) -50 °C, and (c) -75 °C. In this and subsequent figures, the filled points are averages of at least six tests performed on a single specimen, and unfilled points are individual supplementary tests.

done on a single specimen but at increasing stress and strain. These data will be referred to as the principal data. Unfilled points lying one above another on several lines indicate a group of single, supplementary tests performed at different stress rates on a single specimen. The experimental points have been fitted by least squares lines which have been forced through the origin. Their slopes are equal to $\ln R/\Delta\sigma \simeq n/\sigma_e$[4], which is a measure of the semi–logarithmic stress sensitivity of both the strain rate and dislocation velocity, i.e. $d\ln\dot{\epsilon}/d\sigma = d\ln v/d\sigma$. (Recall that in this test, because the mobile density is taken to be unchanged during the stress decrease, the stress sensitivities of the strain rate and dislocation velocity are identical.) Additionally, this fitting procedure provides a useful method of smoothing measured R values, which requires fewer measurements than the technique (used in this study) of averaging several measurements for a single valued stress decrease.

3.2.3 Effects of Stress Rate and Temperature

The variation of slope in Figure 3.6 characterizes the temperature and stress rate dependences of the semi–logarithmic stress sensitivity, as defined by the ratio n/σ_e. To better show these variations, a cross plot (Figure 3.7) is constructed using the fitted slopes *vs* stress rate. At -20 °C, the stress sensitivity is both large and sensitive to stress rate, increasing from 0.10 MPa^{-1}, at 1.0 MPa/s, to 0.37 MPa^{-1}, at 6.6×10^{-3} MPa/s. With decreasing temperature, both the stress sensitivity and the its variation with stress rate decline. For example at -75 °C, the stress sensitivity varies from 0.060 MPa^{-1}, at 1.0 MPa/s, to 0.096 MPa^{-1}, at 6.5×10^{-3} MPa/s.

[4]In the thermal activation literature, $n/\sigma_e = V^*/kT$ where V^* is the activation volume.

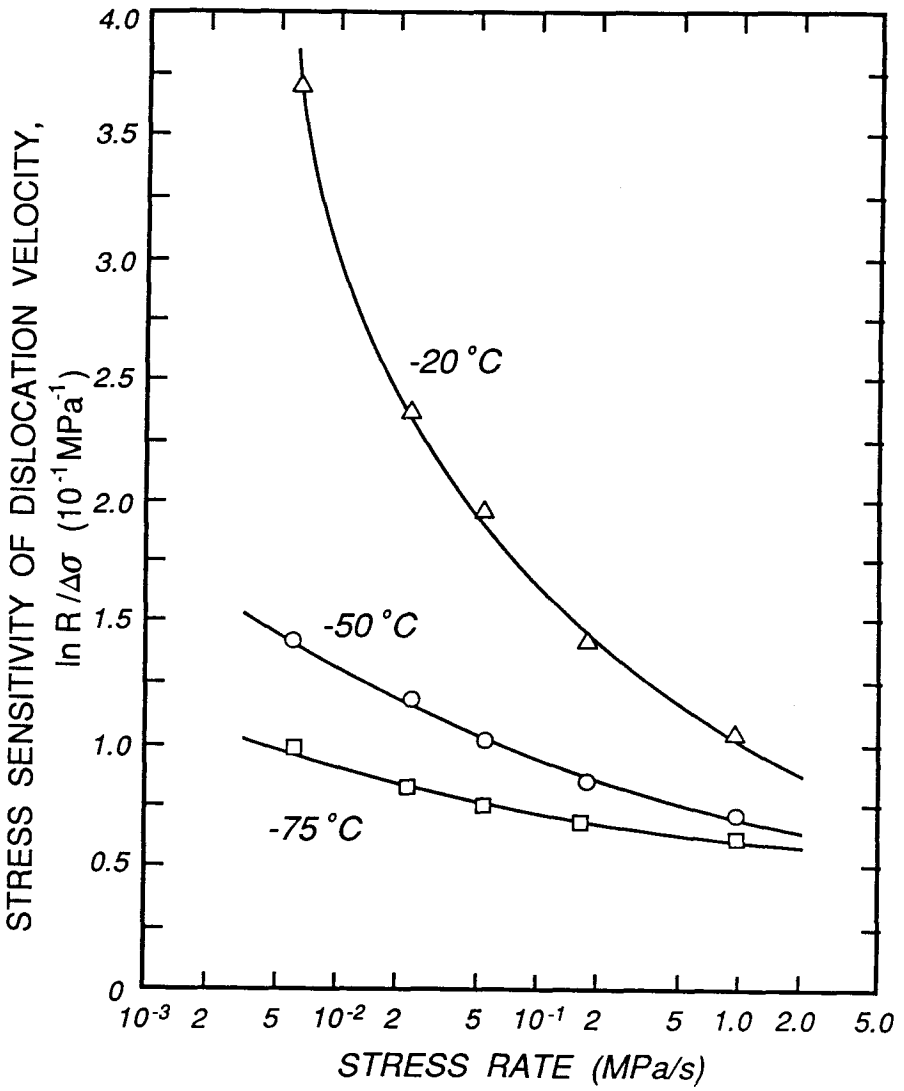

Figure 3.7: Stress sensitivity of the dislocation velocity, as defined by $d\ln v/d\sigma = n/\sigma_e$, *vs* stress rate for three temperatures. Recall that in a stress decrease experiment, because the mobile density is taken to be unchanged during the stress decrease, the stress sensitivities of the strain rate and the dislocation velocity are identical.

3.3 Calculation of Dislocation Velocity Constants

For each temperature, the velocity equation constants, n and τ_o, are determined from a theoretical fit of a strain rate ratio *vs* stress rate profile for a single valued stress decrease, as shown in Figure 3.8. The fits have been made to the principal strain rate ratio data obtained from several tests performed on a single specimen. (Alternatively, fits could have been made to smoothed R *vs* $\dot{\sigma}$ data obtained from the slope of lines in Figure 3.6, for a single valued stress decrease.) The fitted curves are included in Figure 3.8. Although these theoretical curves appear to be continuous, they have been obtained by joining discrete strain rate ratios calculated using a particular stress drop and several stress rates. Then, using the fitted values for n and τ_o, additional theoretical curves are calculated for supplementary stress drops; their good agreement attests to the predictive capability of the model.

Fitting is done by generating a great number of strain rate ratios for each experimental stress rate using a computer program with two nested control loops, which increment separately the values of n and τ_o. Initially, a wide range of n and τ_o values is tried using coarse increments. Then, as the region of possibility in n and τ_o parameter space (which contains the best fit values of n and τ_o) is reduced, finer increments are chosen. Smart choices for n and τ_o are made according to the observation that n and τ_o separately control two aspects of the strain rate ratio: (1) the smaller the value of n, the more sensitive the strain rate ratio will be to stress rate, i.e. the slope of the R *vs* $\dot{\sigma}$ curve is steeper and R increases more rapidly at lower stress rates; and (2) the larger the value of τ_o, the smaller is the strain rate ratio, i.e. the entire R *vs* $\dot{\sigma}$ curve shifts downwards to smaller strain rate ratios, while its slope remains essentially unchanged.

In addition, the best fit values of n and τ_o were determined by minimizing the Chi square (χ^2), which is a weighted least–squares calculation. That is, for each set of n and

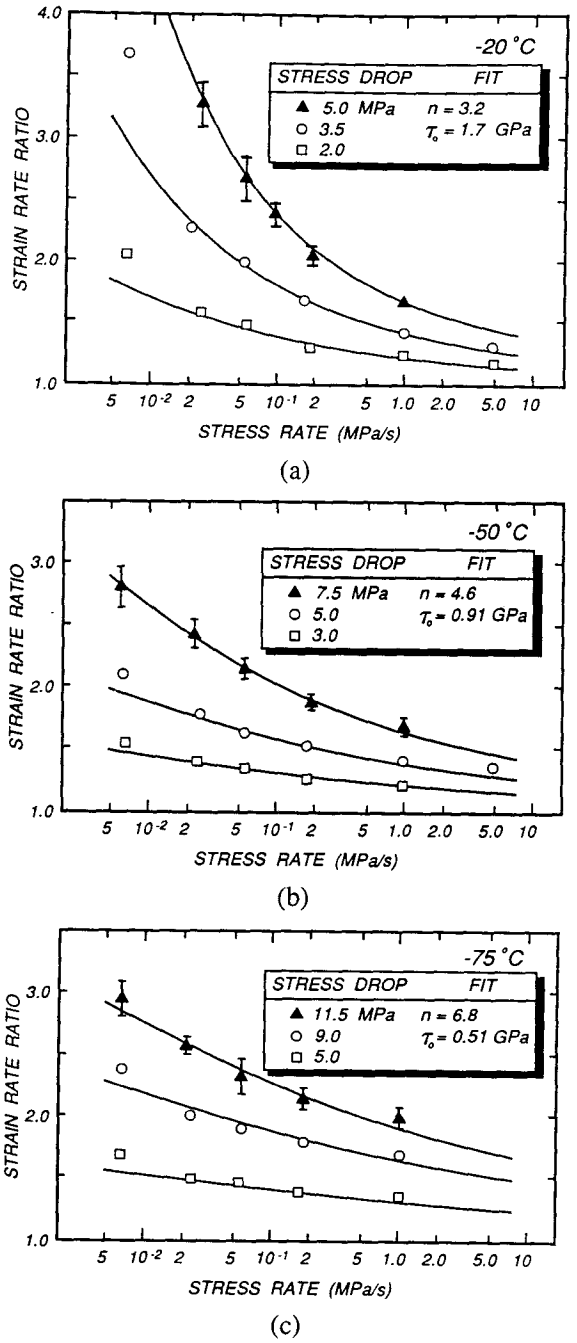

Figure 3.8: Strain rate ratio *vs* applied stress rate for various stress drops at (a) -20 °C, (b) -50 °C and (c) -75 °C. Experimental points, theoretical curves. Theoretical fits have been made to the filled points which are mean values of R for several tests. A scatter bar represents a single standard deviation on either side of the mean R value. Unfilled points represent supplementary single tests of the predictive capabilities of the theory.

τ_o values and a series of calculated R *vs* $\dot{\sigma}$ values, χ^2 is given by the sum of the squares of the weighted residuals between the measured and calculated strain rate ratios; the weights used are the estimated standard deviations of the measured R values at each stress rate:

$$\chi^2 = \sum_{i=1}^{N} \left(\frac{R_i - R(\dot{\sigma}_i; n, \tau_o)}{s_i} \right)^2 \tag{3.29}$$

The best fit of an experimental R *vs* $\dot{\sigma}$ curve produces a minimum χ^2. (A rule of thumb for a moderately good fit is $\chi^2 \approx \nu$ or the *number of degrees of freedom* [46]; in these fits $\nu = N - 2$, where $N = 5$ is the number of R *vs* $\dot{\sigma}$ values being fitted.)

Confidence intervals were also determined by calculating the region bounded by perturbations equal to $\Delta\chi^2 = 1$ away from the best fit values of n and τ_o (Figures 3.9(a-c).) The boundary was calculated by separately incrementing n and τ_o and discarding those values which gave $\Delta\chi^2 > 1$. The projection of the $\Delta\chi^2 = 1$ boundary onto each axis gives the 68.3% confidence interval (two standard deviations wide) for n and τ_o, respectively [46].

The results of this curve fitting exercise, as represented by Figures 3.8 and 3.9 and summarized in Figure 3.10, establish the dynamic constants for IF iron. With decreasing temperature, τ_o declines from 1.7×10^9 Pa at -20 °C to 5.1×10^8 Pa at -75 °C, while n increases from 3.2 to 6.8. The values at ambient temperature are $n = 2.0$ and $\tau_o = 3.6 \times 10^9$ Pa, which were determined previously [3].

It is implicit in the calculation of the strain rate ratio, as it is influenced by the magnitude of the stress decrease and stress rate, that the value of the effective stress is determined simultaneously when the values of n and τ_o have been determined. (This determination can be done because the value of the effective stress is established by the values of n and τ_o and the stress rate. In comparison, the influence of the strain hardening rate, which depends upon the value of the mean free path r_o is negligible.

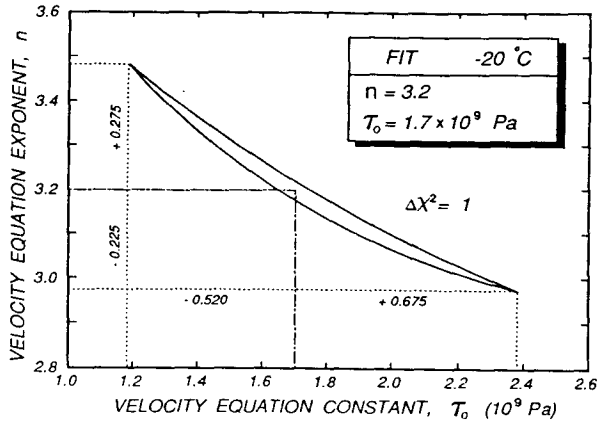

(a)

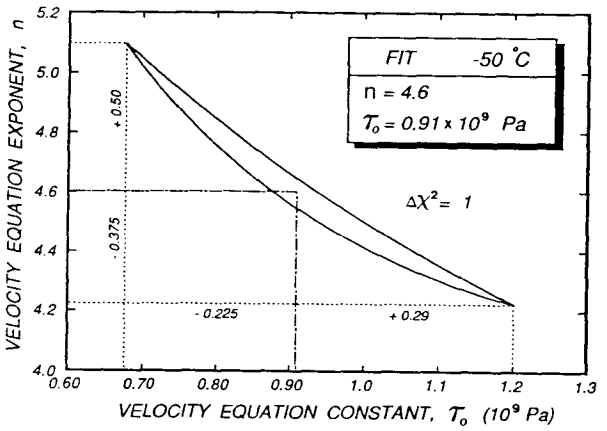

(b)

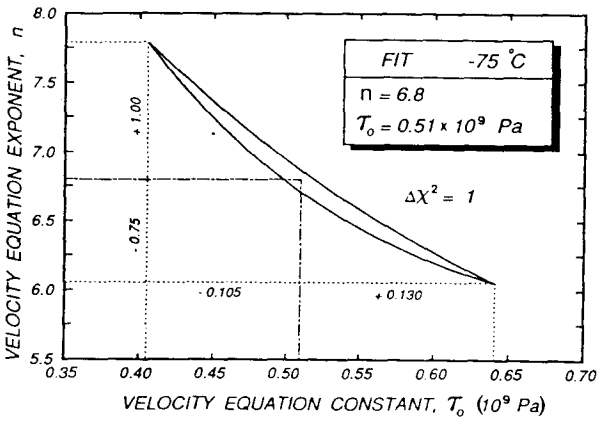

(c)

Figure 3.9: The optimized Chi-squared fit of the dislocation velocity constants and their calculated confidence intervals for (a) -20 °C, (b) -50 °C and (c) -75 °C. The confidence region boundary shown corresponds to $\Delta\chi^2 = 1$ larger than the minimum Chi-squared. The projection of the boundary onto each axis gives the 68.3% confidence interval (two standard deviations wide) for n and τ_o, respectively.

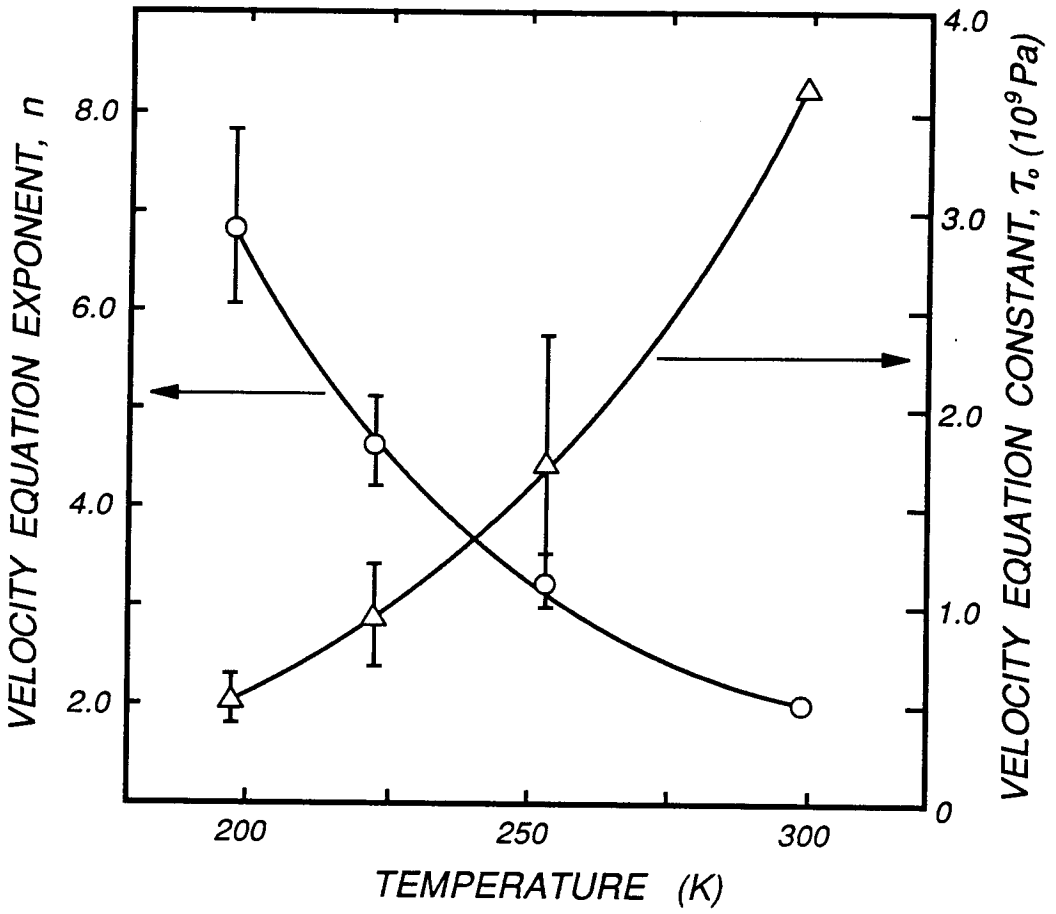

Figure 3.10: Temperature variation of the dislocation velocity constants.

In these simulations, r_o was taken to be the value determined at 25 °C (r_o = 4.5 μm) [3]; doubling this value, for example, increased σ_e by less than 5 %, at 1.0 % strain.) Calculations show that the effective stress will be both small, in comparison to the applied stress, and stress rate sensitive if n is small. In particular, Alden [3] has shown that this is nature of IF iron at 25 °C for which the calculated tensile value of the effective stress is very small (e.g. the theoretical tensile value is only 7.7 MPa at a stress rate of 1.0 MPa/s). This is also the nature of IF iron at -20 °C. Not only is the effective stress small in comparison to the applied stress (albeit about 4.4 times larger than the 25 °C value, at 1.0 MPa/s), but its value is still very much stress rate sensitive, as implied by the strong stress rate dependence of both the strain rate ratio (Figure 3.8(a)) and stress sensitivity of the dislocation velocity (Figure 3.7).

A separate decrease of τ_o will also lower the value of the effective stress. However, despite the declining value of τ_o at low temperature, this effect is overshadowed by the strong temperature dependence of n. For example, the calculated tensile value of the effective stress at -75 °C and a stress rate of 1.0 MPa/s is 116 MPa. In addition, the large n value is responsible for the lowered stress rate depedence of both the strain rate ratio (Figure 3.8(c)) and stress sensitivity of the dislocation velocity (Figure 3.7). (There is a probably a practical upper limit to the value of n which can be determined by application of this technique. This limit will be reached before the stress rate sensitivity of the strain rate ratio becomes vanishingly small.)

3.4 Determination of Static Strength Constants

So far, the theory has been used to calculate the stress sensitivity of the dislocation velocity of IF iron, for several temperatures, as it is influenced by stress rate and the magnitude

of the stress decrease. The success of these predictions require that the dynamic resistance to dislocation glide, which is equal to the effective stress, be calculated from the theory. The theory permits this calculation once the dislocation velocity constants have been determined. The calculation of these dynamic properties depends strongly on neither the nature of strain hardening (e.g. linear *vs* parabolic) nor the value of the strain hardening coefficient. In order to calculate other mechanical properties of IF iron, which depend additionally on the evolution of the network dislocation microstructure, strain hardening must be considered. These properties include the strain *vs* stress curve, the strain rate and its recovery after an abrupt stress decrease, and the strain dependence of the stress sensitivity n^*. (The emphasis of this thesis, however, is not the measurement and prediction of properties which depend primarily on the evolution of the network dislocation microstructure.)

As indicated in Section 3.1, strain hardening in IF iron is apparently more complex than can be described by a simple linear or parabolic hardening law. However, moderately good fits to the strain *vs* stress curve up to about 8.0 % strain (Figure 3.11(a)) can be made using the parabolic hardening law (Eq. 3.24), if the hardening rate is adjusted slightly to account for effects of temperature. The adjustable constant in this fit is the mean free path r_o, which may be calculated directly from the curvature $(dS/d\sigma)$ of the tensile strain *vs* stress curve (Figure 3.11(b)).

To perform this calculation, the strain hardening coefficient[5] is equated to the inverse slope of the strain *vs* stress curve,

$$\theta \simeq \frac{1}{M^2 S}. \tag{3.30}$$

Substituting into Eq. [3.30] an equation for the strain hardening coefficient, which is derived from the theory (Eq. [1.18]), and the empirical equation for the slope of a

[5]The precise statement of the strain hardening coefficient is provided by the derivative of the static strength with respect to strain, $\theta = d\tau_s/d\epsilon$.

parabolic strain *vs* stress curve (Eq. [3.25]), and then rearranging for r_o gives:

$$r_o = \frac{\alpha^2 G^2 b}{k^2}. \tag{3.31}$$

Here, k is the constant in the parabolic hardening law equation (Eq. [3.24]); its shear value can be evaluated from the curvature of a tensile strain *vs* stress curve,

$$\frac{1}{k^2} = \frac{M^3}{2}\left[\frac{dS}{d\sigma}\right]. \tag{3.32}$$

Fitting the curvature of the strain *vs* stress curves, shown by the slope of the light lines in Figure 3.11(b), is not as straight forward as the above discussion implies. Inasmuch as the strain *vs* stress curves do not exhibit well-defined, constant, changes of slope with stress (curvature), there is some uncertainty as to which value of the curvature to choose. (It may be a fact that the increasing curvature of the strain *vs* stress curves indicates that trapping becomes less efficient at higher stresses, and as a result the mean free path increases.) Consequently, in order to make reasonably good fits to the experimental stress *vs* strain curves up to about 8.0 % strain, we take an average of the change of slope with stress over this range of strain, at each temperature. These average curvatures are shown by the solid lines in Figure 3.11(b). The calculated values of r_o, which are summarized in Table 3.3, increase from 4.5 μm to 5.6 μm, as the temperature decreases from -20 °C to -75 °C; at 25 °C, the curvature of the strain *vs* stress curve is consistent with $r_o = 4.5$ μm as determined in the previous room temperature study [3]. These adjustments in the values of r_o do not affect the fits of n and τ_o.

In addition to fixing the values of r_o to account for the increase of static strength due to strain hardening, it is found that in order to fit the experimental strain *vs* stress curves, the calculated strain *vs* stress curves must all be shifted to higher stresses by a constant amount of about 30 MPa (with respect to the shear modulus at 25 °C). This stress which has a shear value of 1.1×10^7 Pa, presumably arises from sources of

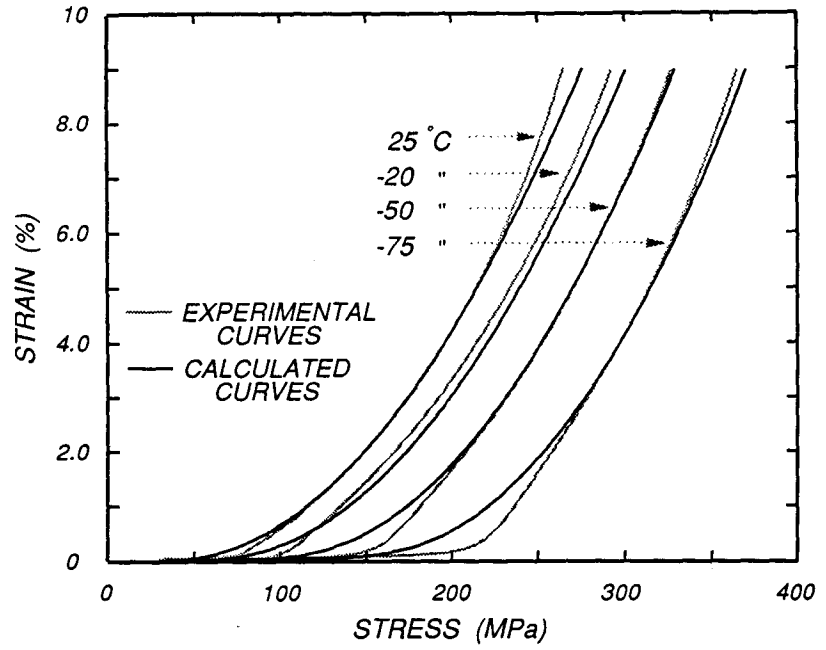

(a)

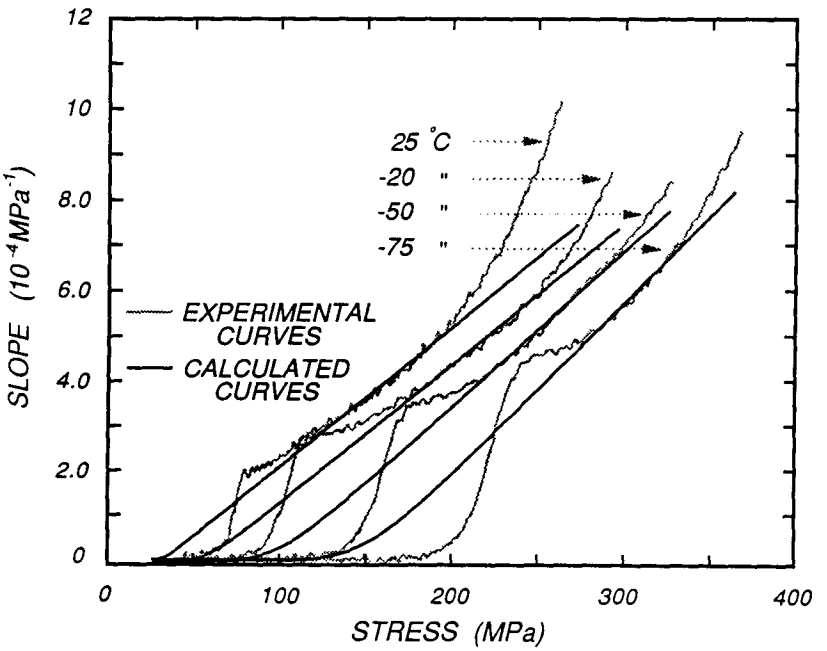

(b)

Figure 3.11: Curve fitting to (a) the strain *vs* stress curves and (b) the slope ($\dot{\epsilon}/\dot{\sigma}$) *vs* stress curves establishes the initial static strength ($\tau^o{}_{ss}$) and the mean free path (r_o) for this material. The curves have been normalized with respect to the 25 °C shear modulus.

static strength in the annealed material, such as grain boundaries, coarse precipitates or clustering of excess titanium or other solute atoms. (Recall that the static strength due to residual dislocations in the recrystallized material has already been roughly accounted for by assuming an initial network density of $\rho_n = 10^9$ m^{-2}, which contributes about 0.5 MPa to the initial tensile strength.) The result of this final curve fitting exercise is shown in Figure 3.11(a).

One final discrepancy between the calculated and experimental strain *vs* stress curves (and unresolved in this study) is the nature of the elastic–to–inelastic transition. While the experimental curves show a rapid elastic–to–inelastic transition, which is indicated by an abrupt rise in strain rate (Figure 3.11(b)), the theoretical curves show a more gradual transition. Moreover, this difference in yield behaviour results in a gap between the larger experimental and the smaller predicted 0.2 % offset yield stress (Figure 3.12). This gap widens as the temperature decreases, but eventually disappears at larger stresses and strains.

In Figure 3.12, the calculated 0.2 % offset yield strength is given by the sum of the dynamic and static components, where the static strength incorporates both the initial static strength and strain hardening (which contributes about 36 MPa at this level of strain). The calculated dynamic strength, which is equal to the effective stress, increases from 7.7 MPa at 25 *°C* to 116 MPa at -75 °C and evidently accounts for the most of the temperature dependence of the experimental 0.2 % offset yield stress. The remaining difference, which is largely temperature independent, is mostly accounted for by the calculated static strength. In comparison, the gap between the experimental and theoretical yield stresses is small. At this time we are not certain as to the origin of this discrepancy. Perhaps, if dislocation sources in the annealed material are slightly pinned, then an extra unpinning stress, which may be temperature dependent, will be required. Then, yielding will be delayed until the unpinning stress is reached; afterwards

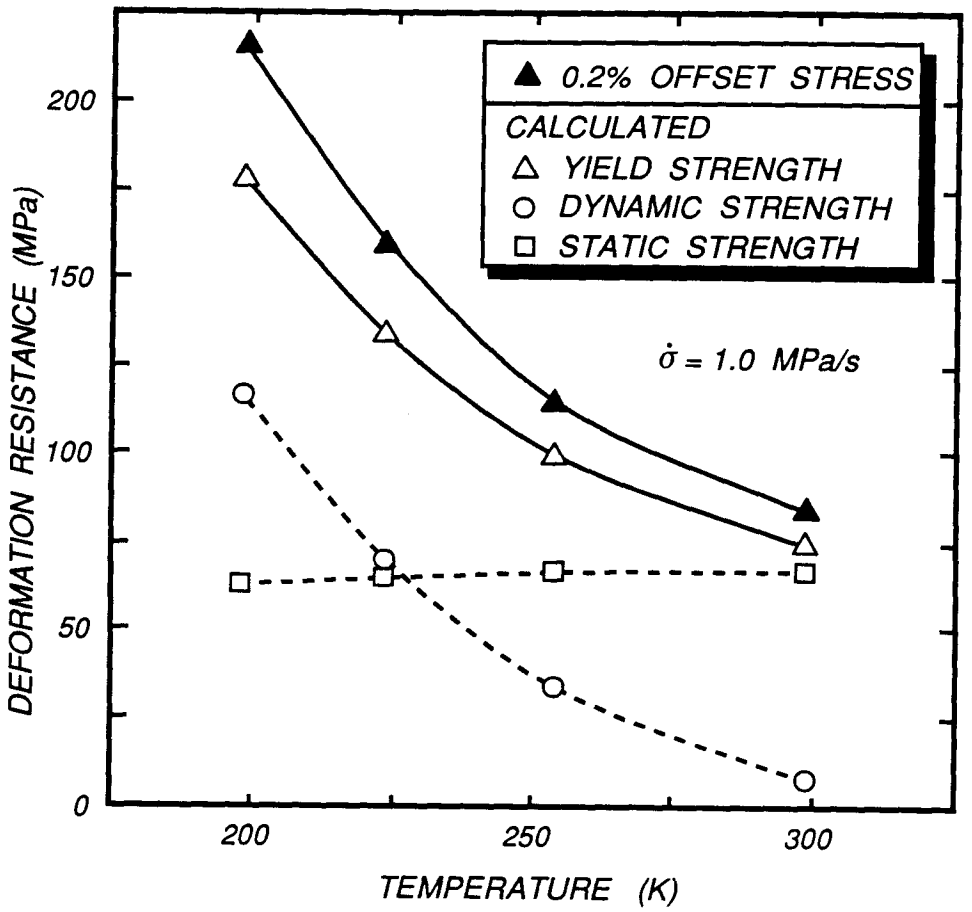

Figure 3.12: Comparison of the measured and calculated 0.2 % yield stresses. The calculated yield strength is given as the sum of both the dynamic and static components. All stress values have been normalized with respect to the 25 °C shear modulus.

Table 3.3: Summary of the fitted constants

Temperature (K)	n	τ_o (Pa)	r_o (m)	$\hat{\tau}_s^o$ (Pa)
298	2.0	3.6×10^{9}	4.5×10^{-6}	1.1×10^{7}
253	3.2	1.7×10^{9}	4.5×10^{-6}	"
223	4.6	9.1×10^{8}	5.0×10^{-6}	"
198	6.8	5.1×10^{8}	5.6×10^{-6}	"

dislocation multiplication may occur, for a short time, at a higher rate than is given by Eq. [1.12]. We note that the resolution of this problem is not the central issue of this study.

The results of these two curve–fitting exercises, as represented by Figures 3.8 and 3.11, and summarized in Table 3.3, establish the deformation constants for IF iron. It is now possible to calculate all of the mechanical and microstructural variables for IF iron. As an example of such calculations, Figures 3.13(a) and (b) show the microstructural parameters which determine the inelastic strain rate and the various components of the deformation resistance (static and dynamic strengths) of IF iron, as they vary with the increase of stress and strain, for a strain *vs* stress test performed at -50 °C and at a stress rate of 1.0 MPa/s. (Recall that in a soft machine test, stress is the independent variable, while strain is the dependent variable. In Figures 3.13(a) and (b), however, strain is plotted on the abscissa so that, in a later discussion, hard and soft machine simulations can be readily compared.) Notice particularly that the dislocation velocity and the dynamic resistance (effective stress) are nearly constant with stress and strain, after a rapid initial increase at small strain. (The values of both the dislocation velocity and the effective stress increase with stress rate, but only the effective stress increases with the values of the dislocation velocity constants (at low temperature), the dislocation velocity declines.) Despite the constancy of the dislocation velocity, the strain rate rises

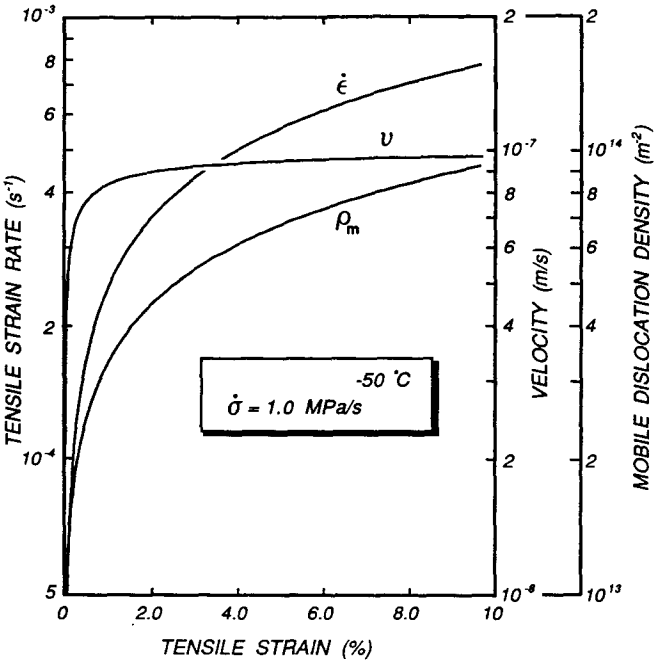

(a)

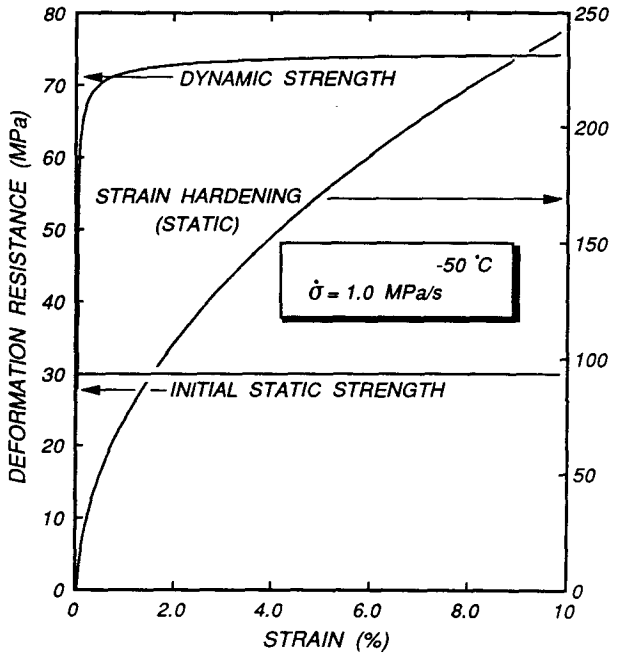

(b)

Figure 3.13: Theoretical predictions of (a) microstructural parameters of the inelastic strain rate, and (b) static and dynamic components of the deformation resistance, for a stress *vs* strain test at -50 °C and 1.0 MPa/s rate of stress increase.

as the mobile dislocation density increases (Figure 3.13(a)).

Strain hardening is the only component of the deformation resistance (Figure 3.13(b)) which increases with stress and strain. The initial static resistance is constant, by definition. (Both components of the static strength, as defined by theory, are also rate insensitive.) The constancy of the effective stress with increasing stress and strain is an important result and underlies the constancy of the strain rate ratio.

3.5 Additional Measured and Simulated Tests

3.5.1 Recovery of Strain Rate

After the abrupt stress decrease, in a soft machine stress drop test, the applied stress continues to rise at a constant rate and the strain rate gradually recovers to its prior maximum value. Both the times and shape of this recovery are of particular interest, and provide a basis on which to test the model's central hypothesis concerning the evolution of the mobile dislocation density [3]. Although several stress drop tests have been performed in procuring values for n and τ_o, separate strain rate recovery tests have been done, primarily because recovery times are long in this material. This tendency causes specimens to suffer appreciable additional strain prior to the recovery of the strain rate. Recovery tests have not been performed at every deformation temperature for which the material constants have been determined. Instead, supplementing tests already performed at 25 °C [3], a few representative tests have been done at -50 °C using a stress rate of 1.0 MPa/s and four stress drops ranging from 2.5 MPa to 10 MPa, or about 3.3 % to 13 % of the calculated effective stress. The stress drops were applied after a prestrain of about 3.0 %, at 225 MPa, at which the model first matches the experimental strain hardening rate (see Figure 3.11(a)).

The results of these experiments show that recovery times of the strain rate are always

much longer than the times required to restore the applied stress to its prior maximum value. For example after a stress decrease of 2.5 MPa, the recovery time of the strain rate is 12.3 s. After a 7.5 MPa stress decrease, the recovery time is 23.0 s (Figures 3.14(a) and (b)). As reported in the prior study [3], these times increase, but not proportionately, with the magnitude of the stress decrease (Figure 3.14(b)). The usual shape of the recovery consists of (1) an initial region of low slope, which ends approximately with the time required to restore the applied stress to its prior maximum value, followed by (2) a region of higher, but falling slope (Figure 3.14(a)). The model makes quantitative predictions of both the shape and times of this recovery.

These quantitative predictions, particularly of the shape of the recovery, provide confirmation of the equations governing the evolution of the mobile dislocation density [3]. Recall that in the theory, the mobile dislocation density is related to the rate of stress increase and not directly the level of stress (or strain) itself. (Perhaps the most persuasive evidence for this hypothesis is from the study of the low temperature creep of 304 stainless steel [5] in which the loading stress rate, used to attain the creep stress, is found to affect strongly the amount of subsequent creep strain.) In the present study, the theory predicts that the mobile density will be unchanged in the instant of the stress decrease. Then, in strict adherence to Eq. [1.11], the total density will not increase again until the applied stress is restored to its prior maximum value. There is a delay time for the generation of new (mobile) dislocations, but the attrition of mobile dislocations to the network (which is the microstructural origin of strain hardening) continues. Because of discontinued generation and continued trapping of mobile dislocations, following the stress decrease, the mobile density declines. Then, at time equal to $\Delta\sigma/\dot{\sigma}$, dislocation generation recommences (Figure 3.15(a)).

The dislocation velocity, on the other hand, falls immediately in response to the stress decrease, but, afterwards, gradually recovers as the applied stress continues to

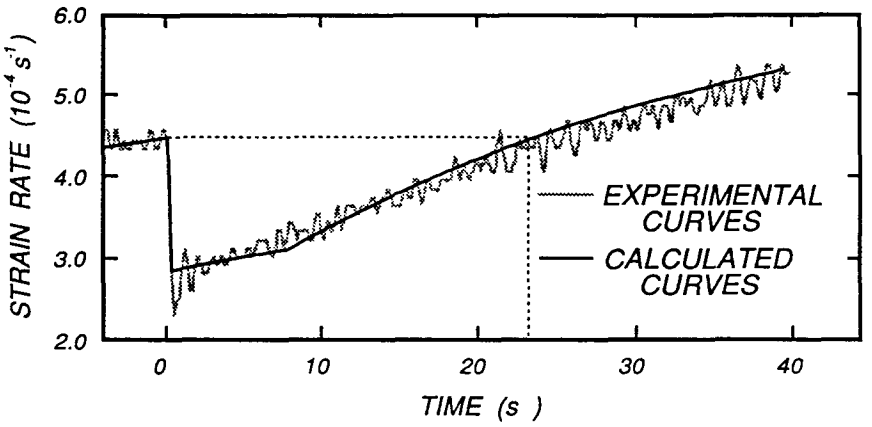

(a)

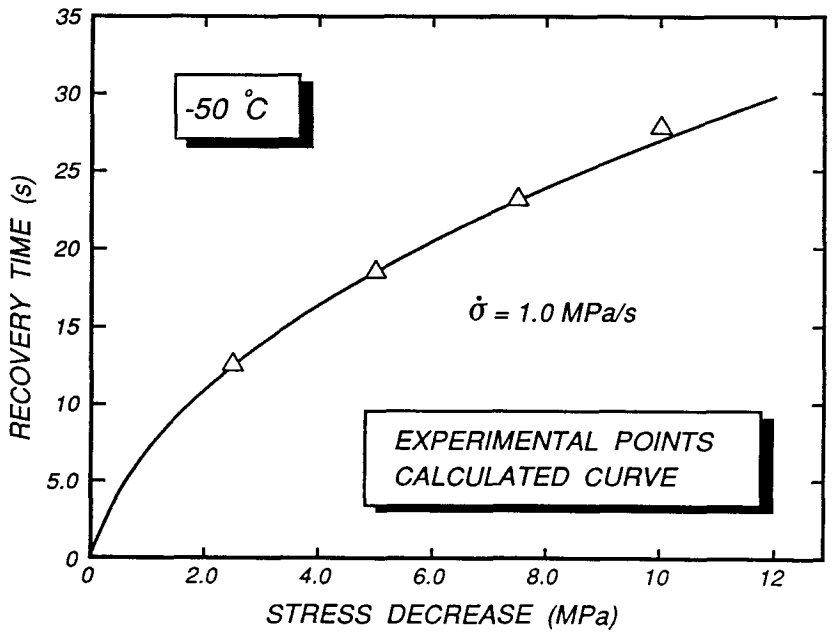

(b)

Figure 3.14: Recovery of strain rate after the abrupt stress decrease. The theory predicts both (a) the initial slow recovery rate and (b) the recovery time. The temperature is -50 °C, stress rate = 1.0 MPa/s and stress = 225 MPa just prior to stress drop. In (a) the magnitude of the stress decrease is 7.5 MPa and the recovery time is 23.0 s.

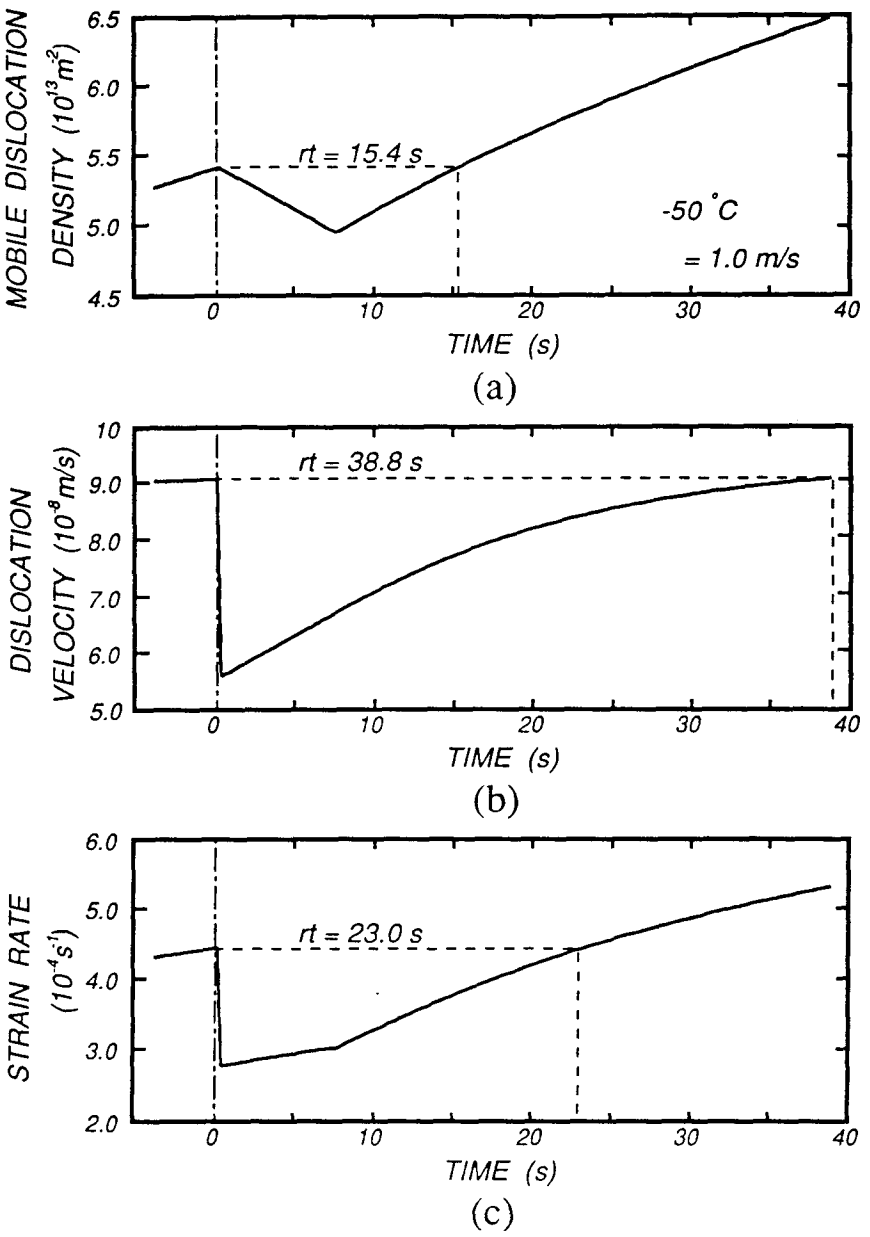

Figure 3.15: Theoretical prediction of the microstructural parameters governing the recovery of the strain rate, following a stress decrease; (a) the mobile dislocation density, (b) dislocation velocity, and (c) inelastic strain rate. The temperature is -50°C, stress rate 1.0 MPa/s, stress 225 MPa and stress drop 7.5 MPa. (The stress continues to rise at constant rate, following the stress decrease.)

rise (Figure 3.15(b)). Despite the continued recovery of the dislocation velocity, the initial recovery of the strain rate will be slow due to the declining mobile density. Once dislocation sources are reactivated, after the delay time, the strain rate rises rapidly to its prior maximum value (Figure 3.15(c)).

3.5.2 Constant Crosshead Speed Tests

Previous tests and simulations were done with the soft tensile machine in which the stress rate is controlled and the extension is measured. In the present section, stress *vs* strain curves are obtained using a conventional hard tensile machine in which the speed of a crosshead is controlled and the load is measured. The control of the crosshead speed makes hard machine tests distinctive in at least two respects:

(1) The stress rate is variable; it depends on the crosshead speed, the elastic deflections of the machine and specimen, and the inelastic deformation of the specimen. For example, in a stress *vs* strain test, the stress rate is high during elastic straining and subsequently declines as inelastic strain increases.

(2) The mobile dislocation density and the dislocation velocity are inextricably linked; an increase in one of these variables requires the decrease in the other. For example, rapid dislocation multiplication at small strain may cause a yield drop in a stress *vs* strain test, or a lessening of the increase of flow stress in an instantaneous upward crosshead speed change test, thereby lowering the measured rate sensitivity.

The primary reason for conducting stress *vs* strain tests at several crosshead speeds and temperature is to obtain experimental curves which can then be compared to theoretical predictions. In particular we are interested in predicitions of the rate sensitivity of IF iron, as indicated by the relative differences between stress levels $\Delta\sigma_f$ of curves obtained for different crosshead speeds, but at constant strain. (A similar, study of the rate sensitivity of the flow stress could have been performed in the soft tensile machine.

but at different stress rates, since the nature of the rate sensitivity of the flow stress does not depend on which testing machine is used.) However, we must note that the measurement of $\Delta\sigma_f$ cannot be used to establish the rate sensitivity of the flow stress, as defined by $m = d\sigma/d\dot{\epsilon}$, primarily because of uncertainty in the constancy of structure. (Recall that in the theory, the total dislocation density depends on the level of stress, and the mobile fraction is determined by a competition between stress rate dependent generation and velocity dependent trapping.) An alternate method would be to perform instantaneous crosshead speed change tests, but even in these tests the constancy of the structure has been questioned [34,36].

Another reason for performing hard machine tests and comparing the results with theory is to demonstrate the versatility of the model in which the stress rate is the central variable controlling the change of structure (Eq. [1.14]). These tests also approximate industrial processes which often impose shape changes at constant rate. However, we note that industrial deformation rates are typically 2 to 5 orders of magnitude greater than the maximum rate which can be attained in the conventional hard testing machine.

Measured Stress versus Strain

Figure 3.16 shows several stress *vs* strain curves obtained at four temperatures (25, −20, −50 and −75 °C) and several crosshead speeds spanning four orders of magnitude (8.5×10^{-4} mm/s to 8.5×10^{-1} mm/s). Observe in this figure that the scales are the same, so that the temperature dependence and rate sensitivity of the flow stresses can be readily compared. The following features are observed:

(1) At small strain, yielding is identified by a stress drop, the magnitude of which increases with crosshead speed and at lower temperature. For example, at ambient temperature and low crosshead speed (8.5×10^{-4} mm/s), the stress drop is vanishingly small. At -75 °C and high crosshead speed (8.5×10^{-1} mm/s), it is about 60 MPa.

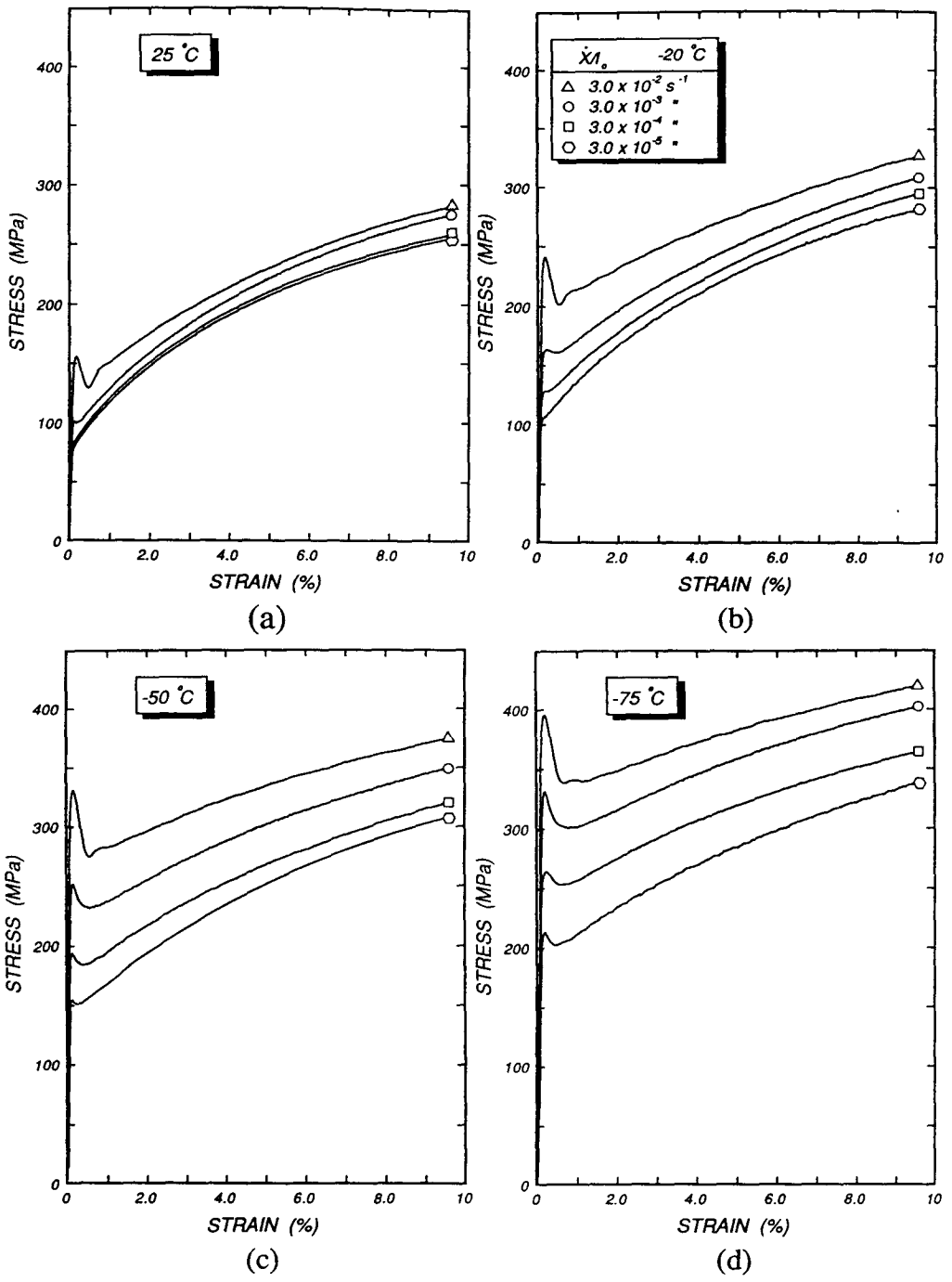

Figure 3.16: Measured hard tensile machine stress *vs* strain curves for four crosshead speeds ($\dot{X}$), ranging from 8.5×10^{-4} to 8.5×10^{-1} mm/s, and at four temperatures: (a) 25 °C, (b) -20 °C, (c) -50 °C and (d) -75 °C. The initial effective gauge length $l_o = 2.86cm$.

As well, the sensitivity of both upper and lower yield stresses to the crosshead speed increases at low temperature.

(2) At strains above about 1.0 %, strain hardening appears to be approximately parabolic. However, the curves cannot be superimposed onto each other by parallel transfer because the strain hardening rate falls with high crosshead speed and low temperature. As a result, the separation between flow stresses of neighbouring curves ($\Delta\sigma_f$), at constant strain, decreases with increasing strain.

(3) The separation between adjacent curves ($\Delta\sigma_f$) is sensitive to crosshead speed and temperature. For example, at 25 °C, $\Delta\sigma_f$ is small and increases successively by a factor of about 2 with each factor 10 increase of crosshead speed. At lower temperature, the magnitude of $\Delta\sigma_f$ increases, but the factor which multiplies successive stress differences diminishes. At -75 °C, the $\Delta\sigma_f$'s are nearly identical between adjacent curves.

Hard Machine Simulations

Simulations of the hard machine tensile tests are similar to those done for the soft machine except, in the hard machine simulation, the stress rate is not explicitly stated but is derived from Eq. [2.23]. Consequently, the model predicts some differences in the microstructural parameters of the inelastic strain rate and levels of effective stress. A typical simulation is done for -50 °C at a crosshead speed of 8.5×10^{-4} mm/s. The mobile density increases with stress and strain. The dislocation velocity, which has a maximum value at small strain, falls in order to maintain a nearly constant but slowly declining strain rate (Figure 3.17(a)). Consequently, the effective stress, which reaches a maximum value at small strain, slowly declines at large strain (Figure 3.17(b)). The strength contributed by strain hardening is assumed to be entirely static, i.e. temperature and rate independent.

The calculated stress *vs* strain curves are presented in Figure 3.18, along with the

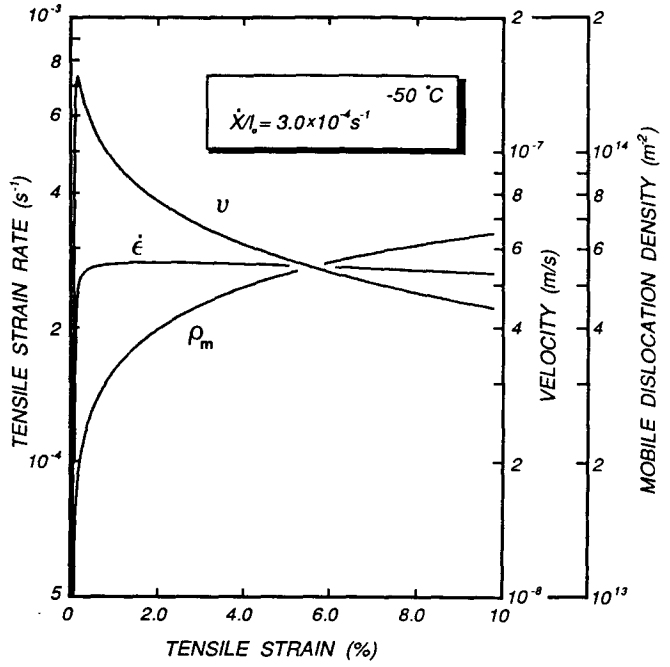

(a)

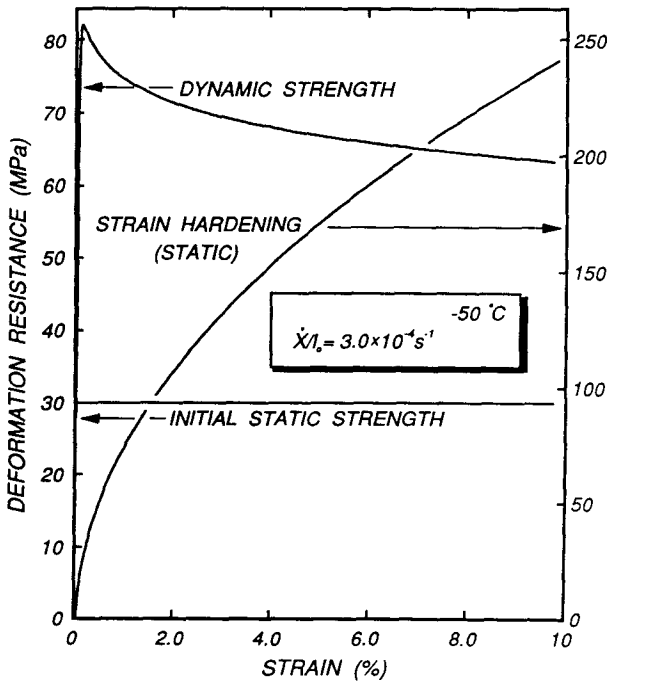

(b)

Figure 3.17: Theoretical predictions of (a) microstructural parameters of the inelastic strain rate, and (b) static and dynamic components of the deformation resistance, for a stress *vs* strain test at -50 °C and a nominal strain rate of 3.0×10^{-4} s^{-1}.

experimental curves for comparison. The differences between the level of the calculated flow stresses, at constant strain, represent only differences in the magnitude of the effective stresses; the calculated static strength, which is indicated by the dashed line, does not vary with crosshead speed (i.e. r_o is assumed to be constant). The theory predicts both the magnitude of the flow stresses and, consequently, the change in effective stress as it varies with strain rate and temperature, particularly at small to moderate strains (Figures 3.18 and 3.19). For example, at 25 °C and 2.0 % strain, the measured stress difference between curves obtained at 3.0×10^{-5} s^{-1} and 3.0×10^{-4} s^{-1} is 3.3 MPa compared to the theoretical value of 3.7 MPa. At -50 °C, the measured stress difference at 3.0×10^{-3} s^{-1} and 3.0×10^{-2} s^{-1} is 41.6 MPa and the theoretical value is 44.8 MPa. (The theory predicts that these values decrease slightly at larger strains due to a falling effective stress (Figure 3.17(b)). However, the decline of the measured stress differences is greater than the theoretical values because of the additional decrease of strain hardening rate with crosshead speed, which the theory does not account for.) At -75 °C, the theory does not predict a constant stress difference for each factor 10 increase of crosshead speed. However, the factor of increase for successive theoretical stress differences is small (approximately 1.3).

Yield Drops

Despite the considerable success of the theory in predicting stress differences, there are two notable differences between the experimental and theoretical stress *vs* strain curves. One discrepancy is the failure of the model, as already noted, to predict yield drops. Instead, the calculated curves rise continuously with stress and strain because the theory assumes that there is always a sufficient number of operable sources for the dislocation density to increase according to Eq. [1.11]. However, in order for there to be a stress drop, there must be a deficiency of dislocation sources in the early stages of strain; for

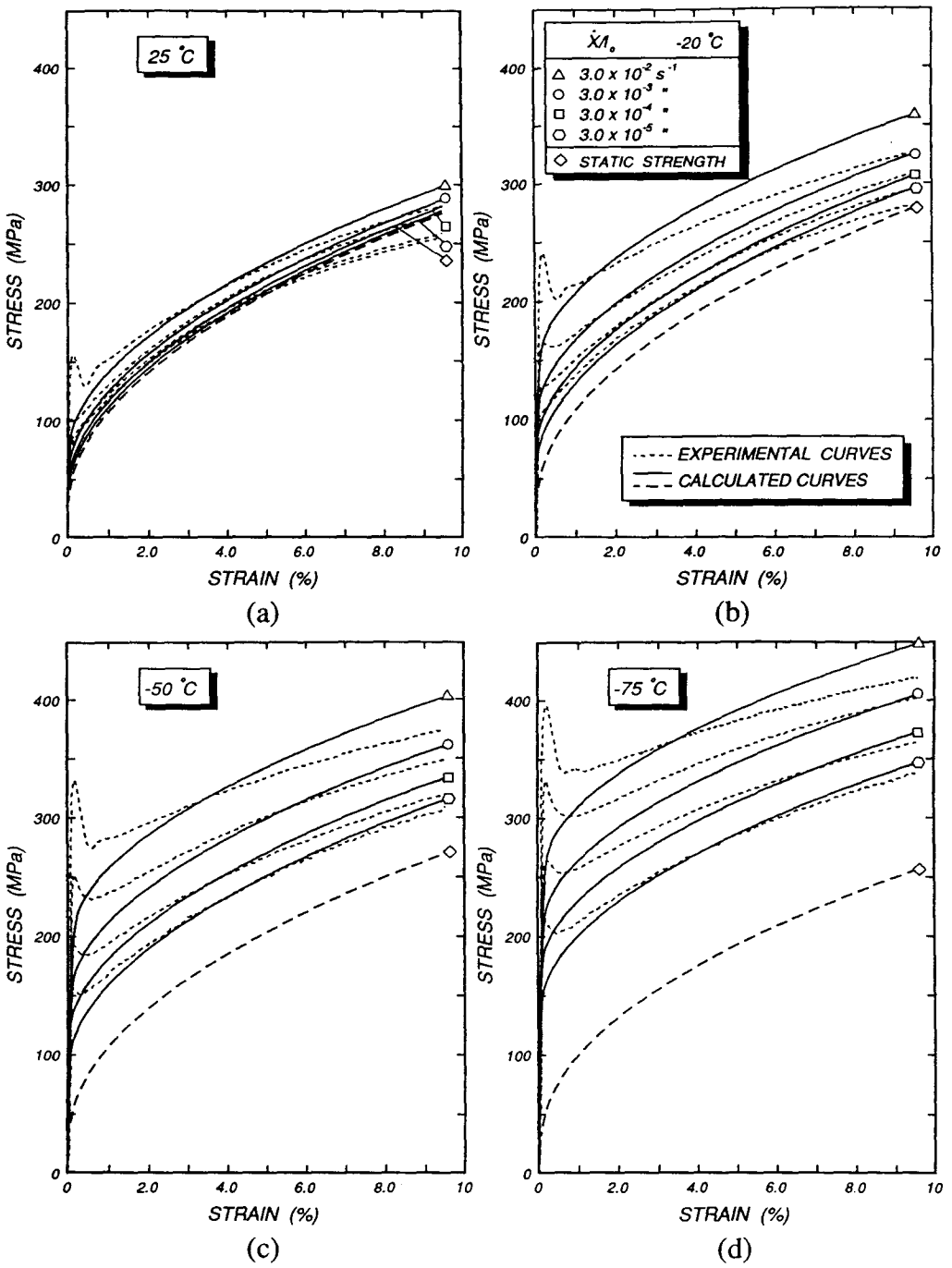

Figure 3.18: Comparison of measured and calculated hard tensile machine stress *vs* strain curves for four crosshead speeds ranging from 8.5×10^{-4} to 8.5×10^{-1} mm/s, and four temperatures: (a) 25 °C, (b) -20 °C, (c) -50 °C and (d) -75 °C. The light dashed lines show measured curves, while the heavy solid lines show the results of model calculations. The calculated static strength is rate insensitive, by definition, and is indicated by the heavy dashed line.

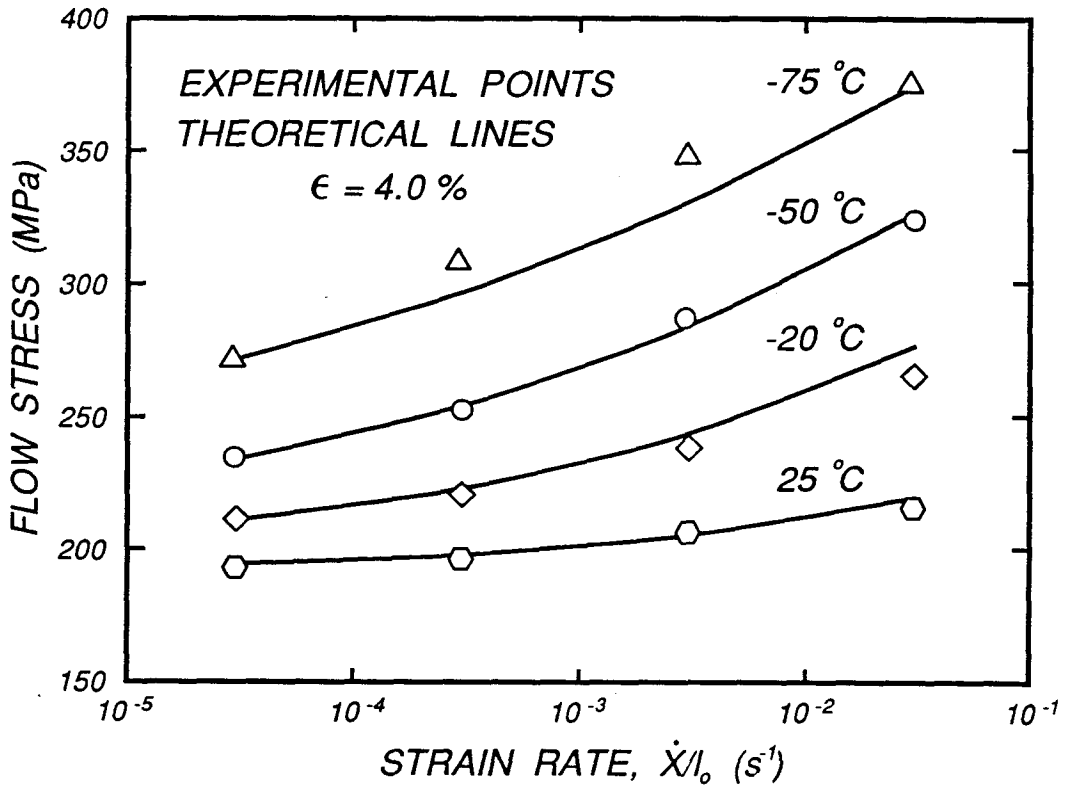

Figure 3.19: Temperature and strain rate dependences of the measured and theoretical flow stresses, at 4.0 % strain.

instance, sources may be pinned by impurity atoms. Note that in the present theory, the mobile density rises very rapidly at small strain (Figure 3.17(a)). Alden [37] has suggested that the theory may be modified by relaxing Eq. [1.11], in the early stages of strain, so that the total dislocation density falls behind its "natural" value (Eq. [1.11]). Once sources are activated, then rapid multiplication may follow, making up the shortfall in total density and causing a temporary drop in stress. Conceptually, the yield drop effect may be included, but the details of the necessary modifications have yet to be worked out.

Strain Hardening

The second difference is between the measured and calculated slopes of the stress *vs* strain curves. Although the strength contributed by strain hardening may be entirely static in nature, the strain hardening rate ($d\sigma/d\epsilon$) falls with increasing crosshead speed and decreasing temperature, i.e. with increasing flow stress. This discrepancy is particularly noticeable for the high crosshead speed tests. However, better agreement is found between experimental and theoretical slopes of the low crosshead speed tests. In particular, for tests performed at crosshead speed $\dot{X} = 8.5 \times 10^{-4}$ mm/s, the strain rate and flow stresses are comparable to those developed in soft machine tests at 1.0 MPa/s. This agreement, however, is expected since it was the slope of the 1.0 MPa/s strain *vs* stress curves that was used to quantify the strain hardening rate (i.e. select r_o).

To explain the temperature and strain rate dependence of the strain hardening rate, we suggest that trapping by stable attractive junction formation may become less efficient at high flow stresses. Consequently, in a material such as iron, in which the friction stress (effective stress) is strongly temperature and rate sensitive, strain hardening will be weaker at low temperature and high strain rate (or stress rate) than at ambient temperature or slow strain rate. (This is contrary to the usual observation, that the net

hardening rate is weaker at the high temperature and slow rate because of the onset of a competitive thermal softening process, e.g. dynamic recovery.) In order to match the weaker strain hardening at high flow stresses, the mean free path (r_o) must increase. For example, to make a good fit to the slope of the experimental curve at -75 °C and a crosshead speed of 8.5×10^{-1} mm/s, the value of r_o must be increased from 5.6 μm (Table 3.3) to about 10 μm.

Unless adjustments in the values of r_o are made to better characterize strain hardening at high crosshead speed, a comparison of the measured and calculated flow stresses will be complicated by the observed rate dependence of the strain hardening rate. However, the difference between flow stresses of adjacent stress *vs* strain curves, at constant strain, may be compared in order to show variations in effective stress. The reasons for this conclusion are twofold: (1) the microstructural origins of the dynamic and static strengths are different, and therefore the magnitude of the dynamic strength is not affected by the magnitude of the static strength (Eq. [1.1]); and (2) it appears that differences in the static strength between adjacent stress *vs* strain curves are small, at small to moderate strains.

Effective Stress

Another comparison of flow stress differences is sometimes made between the so called athermal plateau stress, measured at and above ambient temperature, and the yield stress at lower temperature. In such a comparison the stress difference is used to estimate the effective stress at the lower temperature; strain hardening is taken to be similar between 0 and 0.2 % strain. However, in this material the value of the *effective stress* at ambient temperature is small but not zero. In particular, at 25 °C, 3.0×10^{-5} s^{-1} and 0.2 % offset strain, the theoretical value of the effective stress is 4.72 MPa (at 25 °C. If this value is close to the actual value of the effective stress, then it represents only 5.4 % of the

flow stress; the residual stress is presumably static. Consequently, if one assumes thst the entire yield stress for this test (87.2 MPa) is static, a small, if detectable, error is introduced into the estimation of the effective stress at lower temperature. The estimated effective stresses are shown in Figure 3.20 along with values calculated from the theory. Close agreement is found between theoretical and estimated values of the effective stress, at 25 °C and -20 °C. However, increasing discrepancies as large as about 50 MPa are found at lower temperature and higher strain rate tests. The magnitude of these discrepancies increases with the size of the yield stress drop. Notice in particular, that the larger the yield drop, the greater is the strain at which the lower yield stress is determined. For instance, at -75 °C and 3.0×10^{-3} s^{-1}, the lower yield stress is determined at about 0.6 % inelastic strain; at 3.0×10^{-5} s^{-1}, the strain is about 0.3 %. Consequently, part of the discrepancy between the estimated and theoretical values of the effective stress may be associated with differences in levels of strain hardening.

The Nature of the Rate Sensitivity Behaviour

By definition, the semi–logarithmic strain rate sensitivity of the flow stress at constant structure is given by

$$m' = \frac{d\sigma}{d\ln\dot{\epsilon}} = \frac{\sigma_e}{n}; \tag{3.33}$$

which is the inverse of the semi–logarithmic stress sensitivity of the dislocation velocity. Consequently, the flow stress is rate sensitive if the ratio, σ_e/n, is large (e.g. small n and large τ_o). Conversely, the flow stress is rate insensitive if the ratio, σ_e/n, is small (e.g large n or small τ_o). However, if only n were known, then the rate sensitivity behaviour of IF iron would appear not to follow these rules. For example, despite a small value of n at ambient temperature, the sensitivity of the flow stress is small, as indicated by the small difference between flow stresses in Figure 3.18(a). Then, at lower temperature,

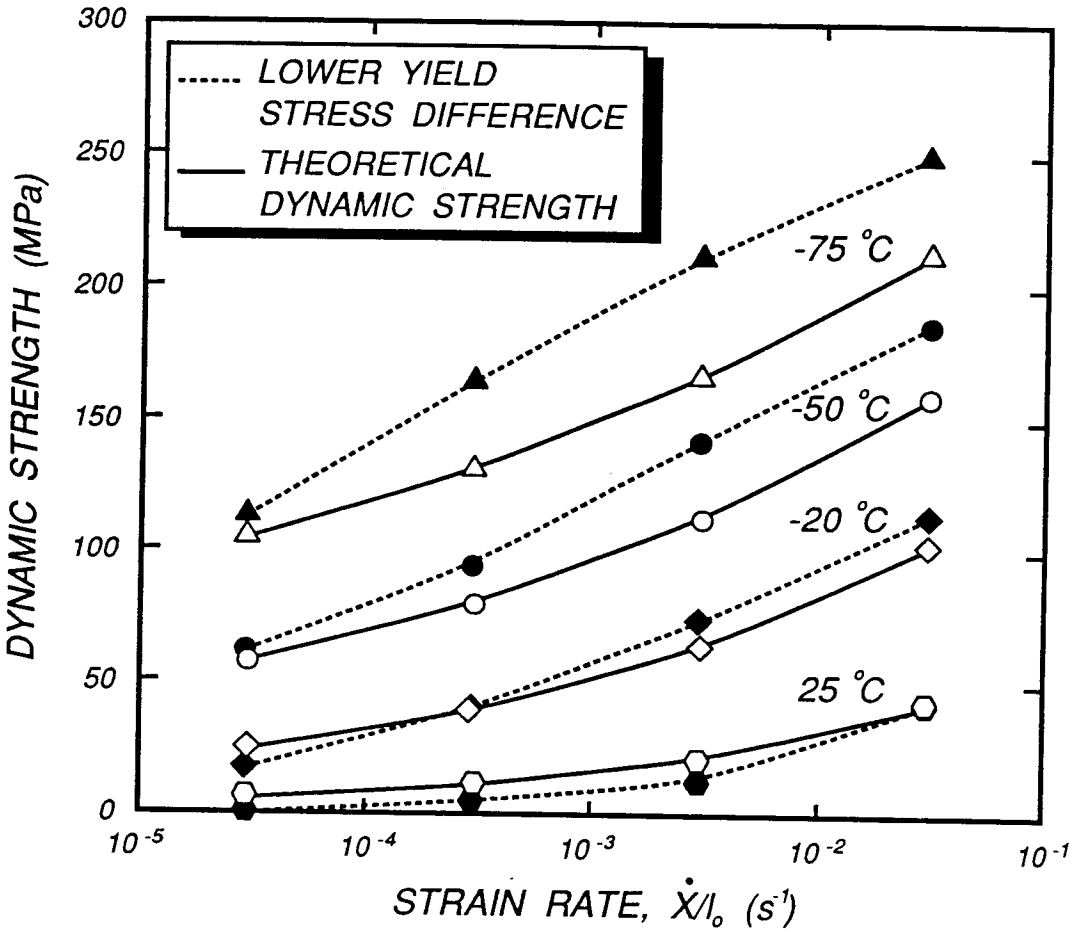

Figure 3.20: Comparison of the estimated and calculated values of the effective stress as they vary with temperature and strain rate. The estimated values are given by the increases of yield stress at low temperature in comparison to the yield stress at 25 °C.

the sensitivity increases (Figures 3.18(b-d)), despite an increasing value of n (Table 3.3). The reason for this discrepancy is the strong temperature dependence of the effective stress, which dominates the rate sensitivity behaviour of IF iron.

It is useful for this discussion to rearrange Eq. [3.33] to give the fractional change of the effective stress accompanying a change of strain rate,

$$\frac{\Delta\sigma}{\sigma_e} = \frac{\ln R}{n} \tag{3.34}$$

At ambient temperature, the *fractional* change of the effective stress may be large, because of a small value of n, but the magnitude of the change of flow stress is small since the effective stress has a small value (Figure 3.20). At lower temperature, the fractional change of the effective stress declines, because of a large value of n, but the magnitude of the stress change will be large as the effective stress increases strongly with declining temperature.

Variation of Microstructural Variables with Declining Temperature

The strong temperature dependence of the effective stress also suggests variations in the values of the microstructural variables. As the temperature decreases, the frictional drag on moving dislocations increases. Then as a result of the theory, the dislocation velocity decreases and the mobile dislocation density increases (at constant strain rate). These predictions are not intuitively obvious because of an increase of flow stress at lower temperature. For an example, theoretical values of the effective stress, dislocation velocity and mobile density are obtained at 2.0 % strain, 3.0×10^{-4} s^{-1} and various temperatures (Table 3.4). At -75 °C, the effective stress is about 17 times larger than at ambient temperature, the dislocation velocity about 10 times smaller, and the mobile density 10 times greater. Unfortunately, it is not possible to directly verify these predictions.

Table 3.4: Calculated mechanical and microstructural variables. $\epsilon = 2.0$ %, nominal $\dot{\epsilon} = 3.0 \times 10^{-4}$ s^{-1}.

Temperature (K)	Stress (MPa)	Effective stress (MPa)	Dislocation velocity (m/s)	Mobile density (m^{-2})
298	150	7.08	5.11×10^{-7}	6.06×10^{12}
253	177	31.4	1.30×10^{-7}	2.38×10^{13}
223	210	70.7	7.47×10^{-8}	4.16×10^{13}
198	256	121	5.93×10^{-8}	5.26×10^{13}

Chapter 4

Further Discussion

4.1 Summary of Results

In this present study we have extended an earlier ambient temperature investigation [3] to measure and predict the dynamic properties of IF iron at three temperatures, -20, -50 and -75 °C. These properties include: (1) the stress sensitivity of strain rate, as is influenced by stress, stress rate and the magnitude of the stress decrease; (2) the nature and recovery time of the strain rate following a stress decrease; and (3) the relative level of hard machine stress *vs* strain curves as a function of crosshead speed.

In order to make predictions of these results, it is necessary to know the dislocation velocity and mobile density as functions of the stress rate, stress and time. The theory permits the calculation of these values providing that the material constants are known, which are descriptive of the dynamic resistance opposing the movement of mobile dislocations and their mean distance of travel prior to being lost to the dislocation network. In conjunction with measurements of the stress sensitivity of the strain rate, we first obtain the primary constants, n and τ_o, which establish the dislocation velocity and the magnitude of the effective stress. Then, from a fit of the strain *vs* stress curve, the secondary constants are obtained which establish the strain hardening rate (r_o) and the initial static strength (τ_s^o).

A principal result of this work may be summarized in a theoretical plot of dislocation velocity *vs* effective stress (Figure 4.21). The value of n establish the slope of the lines.

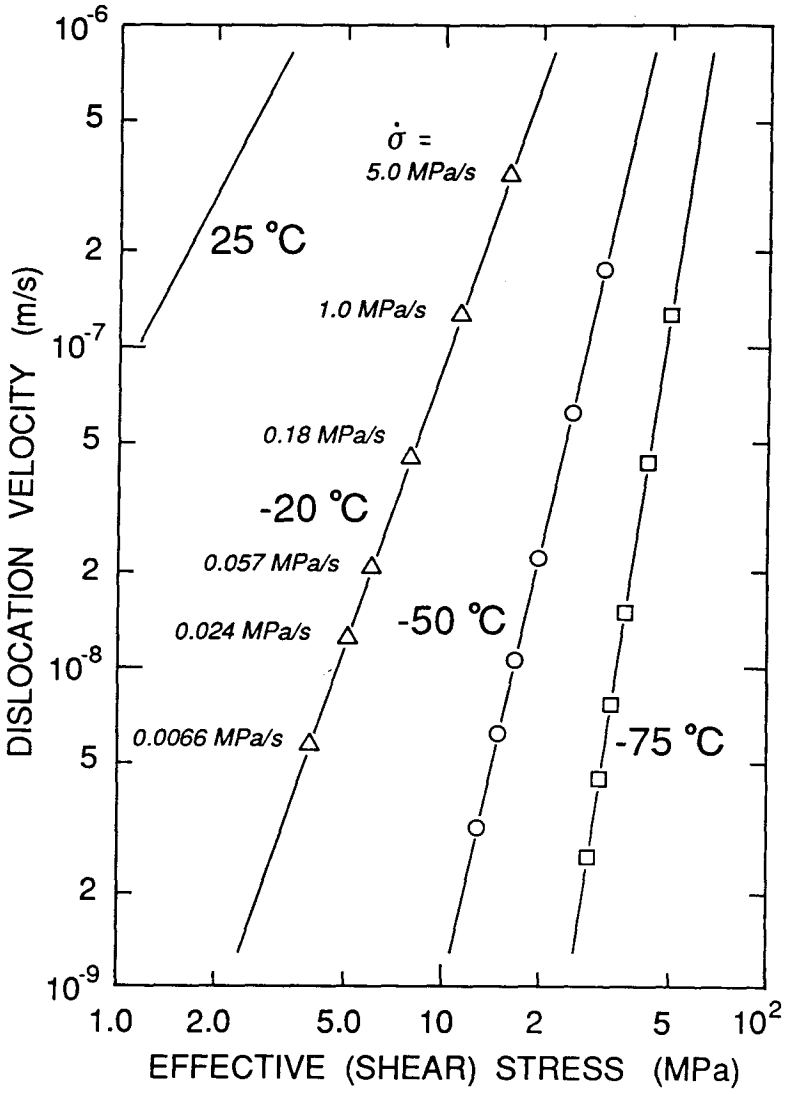

Figure 4.21: Dislocation velocity *vs* effective (shear) stress as determined by experiment and theory.

and τ_o the relative position. The value of n increases from 2.0, at ambient temperature, to 6.8, at -75 °C. The value of τ_o actually declines with falling temperature, from 3.6 $\times$ 10^9 Pa to 5.1 $\times$ 10^8 Pa. The value of the frictional resistance on moving dislocations (dynamic strength) increases as the temperature decreases; this result is shown by the larger effective stresses required to move dislocations and a tendency for the dislocation velocity to fall. At larger effective stress (low temperature and high deformation rate), the model also predicts that mobile dislocation density tends to increase, relative to similar tests done, say, at higher temperature.

4.2 Comparison with Prior Study

The values of the dislocation velocity constants determined in this study are yet to be confirmed by direct methods. Presently, the only available direct determination of the mobility of dislocations in iron is the study done by Turner and Vreeland [17], who measured the velocity of individual edge dislocations in high purity iron using an X-ray method. Their findings are shown in Table 4.5. The values of n are low and less sensitive to temperature, in comparison to the values obtained in this study (Table 3.3). The directly measured values of τ_o are within the same order of magnitude as the values determined in this study, but Turner and Vreeland's τ_o values increase with decreasing temperature over the same range of temperatures for which the values, obtained in this study, decrease.

Using Turner and Vreeland's constants, various mechanical and microstructural variables at 2.0 % strain were calculated for hard machine stress *vs* strain curves at a nominal strain rate equal to 3.0 $\times$ 10^{-4} s^{-1} (Table [4.5]). At ambient temperature, the effective stress, dislocation velocity and mobile density are comparable to the values calculated using the results from the previous study [3] and shown in Table [3.4]. In particular the

Table 4.5: Calculated mechanical and microstructural variables using dislocation velocity constants determined by direct methods for edge dislocations[17]; $\epsilon = 2.0$ %, nominal $\dot{\epsilon} = 3.0 \times 10^{-4}$ s $^{-1}$.

Temperature (K)	n	τ_o (Pa)	σ (MPa)	σ_e (MPa)	v (m/s)	ρ_m (m^{-2})
373	2.56		—	—	—	—
295	2.8	3.0×10^{8}	149	5.45	7.87×10^{-7}	3.93×10^{12}
198	2.97	1.36×10^{9}	156	21.4	2.18×10^{-7}	1.43×10^{13}
77	7.35	3.14×10^{8}	—	—	—	—

value of the effective stress using Turner and Vreeland's constants is slightly smaller than the value calculated from our constants, by the ratio of 5.45/7.08. At 198 K, however, this ratio is 21.4/121. Consequently, Turner and Vreeland's constants are not charater-istic of the strong temperature dependence of the effective and flow stresses observed in IF iron.

It is known, however, that the mobility of edge dislocations is higher than screw dislocations. For instance the velocity in impure LiF [4] was determined to be 50 times higher for edge dislocations. Furthermore, from studies of microstrain, the long-range motion of edge dislocations has been associated with the microyield stress [47]. The motion of screws is then required for macroyielding. Consequently, the mobility of slower moving screw dislocations will determine the strain rate at large strains and, apparently, the dislocation velocity constants determined in this study are for screw dislocations. In Figure 4.22, the weak temperature dependence of the effective stress, calculated at 0.2 % offset strain using Turner and Vreeland's edge constants, agrees well with the temperature dependence of the microyield stress, measured in a prestrained IF iron [47]. (The elastic limit stress in this material is less than 30 MPa.) This behaviour contrasts with the strong temperature dependence of both the the measured macroyield and the calculated effective stresses, using the dislocation constants determined in this study.

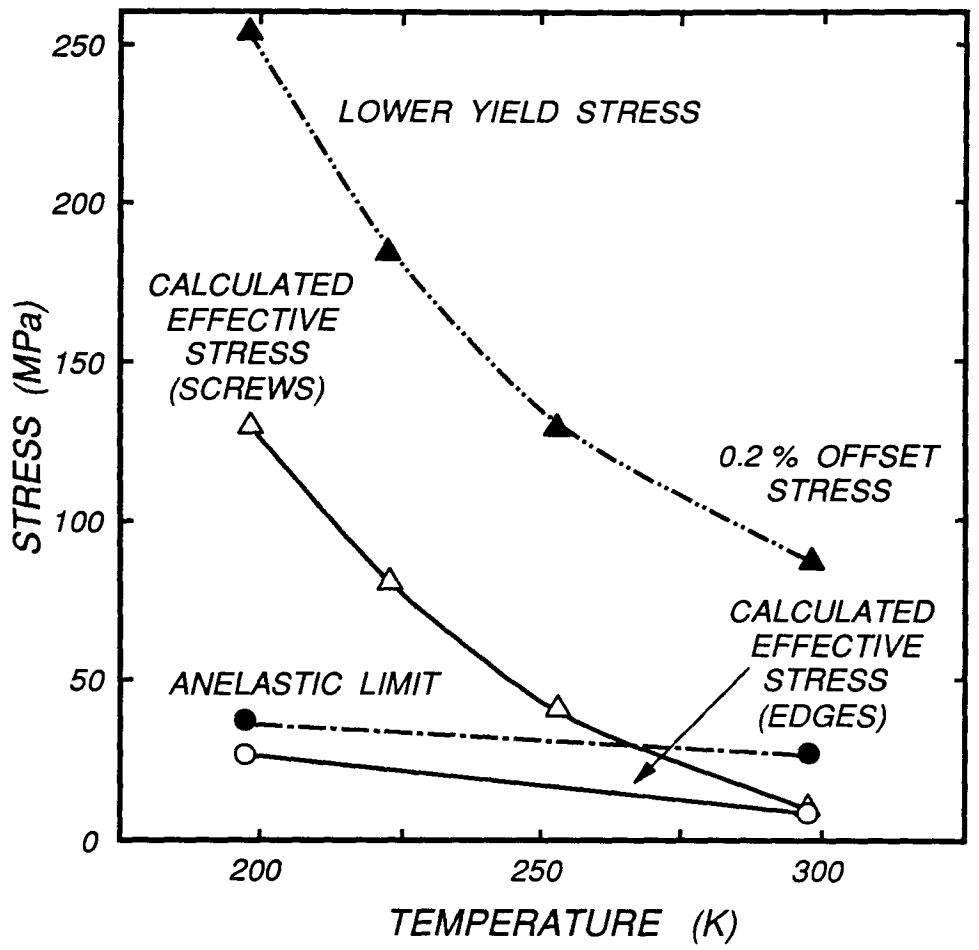

Figure 4.22: Comparison of the calculated effective stresses (0.2 % offset) and the yield stresses associated with the long range motion of edge and screw dislocations. $\dot{\epsilon} \approx 3.0 \times 10^{-4}\ s^{-1}$.

Chapter 5

Conclusions

With modest effort, in comparison to what has been required previously, we have obtained constants of a power–law relationship between the dislocation velocity and effective stress for IF iron at three temperatures, -20, -50 and -75 °C. These determinations supplement an earlier room temperature study [3] of the identical metal, for which the method of analysis was developed. Theoretical predictions of the dynamic properties, based on these results, show excellent quantitative agreement with experiment. Consequently, the theory provides some understanding of the inelastic deformation behaviour of IF iron:

(1) The strong increase of the effective stress below ambient temperature is associated with an increasing value of n; the theoretical value of τ_o actually declines.

(2) The rate sensitivity of the flow stress is linked to the ratio $\sigma_x e/n$. At 25 °C, the sensitivity of the flow stress of IF iron is small, despite a small value of n, since the effective stress is small (e.g. a theoretical tensile value of only 7.1 MPa at 2.0 % strain and a nominal strain rate of 3.0×10^{-4} s^{-1}). At lower temperature, the rate sensitivity increases despite an increasing value of n because of the strong increase of the effective stress (e.g. at -75 °C, the theoretical value is 121 MPa).

(3) The fractional change of the effective stress $\Delta\sigma/\sigma_e$ accompanying a change of strain rate is inverse to the value of n. At 25 °C, the fractional change is large because of the small value of n. At lower temperature the fractional change declines as the value of n increases.

(4) The weak temperature dependence of the effective stress, calculated for the long

range motion of edge dislocations, correlates well with the small temperature dependence of the microyield stress. This behaviour contrasts with the present theoretical prediction of the strong temperature dependence of the macroyield stress, suggesting that the dislocation constants determined in this study are for screw dislocations.

(5) Strain hardening in this metal is generally weaker than parabolic hardening and therefore cannot be characterized by a single valued mean free dislocation path, r_o. (The theoretical value of r_o is only approximately constant below about 8.0 % strain; at larger strains r_o increases.) The observed decrease of the hardening rate with temperature and increasing strain rate (or stress rate) is linked to strong temperature and rate dependence of the flow stress; at higher stresses, the trapping of mobile dislocations may be less efficient.

One shortfall of the theory, in its present form, is its failure to predict a yield drop. However, this phenomenon may not be conceptually excluded if, for example, the number of initially operable dislocation sources in the annealed material is reduced to a small number by dislocation pinning.

References

[1] W. C. Leslie, *Metall. Trans.* **3**, 5 (1972).

[2] W. C. Leslie, R. J. Sober, S. G. Babcock, and S. J. Green, *Trans. ASM* **62**, 690 (1969).

[3] T. H. Alden, *Metall. Trans.* **20A**, 1029 (1989).

[4] W. .G. Johnston and J. J. Gilman, *J. Appl. Phys.* **30**, 129 (1959).

[5] T. H. Alden, *Metall. Trans.* **18A**, 51 (1987).

[6] T. H. Alden, *Metall. Trans.* **18A**, 811 (1987).

[7] H. Conrad, *J. Metals*, 582 (1964).

[8] J. C. M. Li, in *Dislocation Dynamics*, A. R. Rosenfield, et al., (eds.), pp. 87-116, McGraw-Hill, New York (1968).

[9] K. Ono, *J. Appl. Phys.* **39** 1803 (1968).

[10] J. W. Christian, *2nd Int. Conf. on the Strength of Metals and Alloys* **1**, 31, ASM, (1970).

[11] A. S. Krausz and B. Faucher, *Reviews on the Deformation Behaviour of Materials* **6**, 105, (1982).

[12] E. Orowan, *Proc. Phys. Soc. (London)* **52**, 8 (1940).

[13] W. G. Johnston, *J. Appl. Phys.* **33**, 2716 (1962).

[14] H. W. Schadler, *Acta metall.* **12**, 861 (1964).

[15] H. L. Prekel and H. Conrad, *Acta metall.* **15**, 955 (1967).

[16] H. L. Prekel, A. Lawley and H. Conrad, *Acta metall.* **16**, 337 (1968).

[17] A. P. L. Turner and T. Vreeland, Jr., *Acta metall.* **18**, 1225 (1970).

[18] D. F. Stein and J. R. Low, Jr., *J. Appl. Phys.* **31**, 362 (1960).

[19] H. D. Guberman, *Acta metall.* **16**, 713 (1968).

[20] D. P. Pope, T. Vreeland and D. S. Wood, *J. Appl. Phys.* **38**, 4011 (1967).

[21] R. W. Rhode and C. H. Pitt, *J. Appl. Phys.* **38**, 876 (1967).

[22] W. F. Greenman, T. Vreeland, Jr., and D. S. Wood, *J. Appl. Phys.* **38**, 3595 (1967).

[23] K. M. Jassby and T. Vreeland, *Phil. Mag.* **21**, 1147 (1970).

[24] T. Suzuki and T. Ishii, *Proc. Int. Conf. on Strength of Metals and Alloys*, Trans. JIM **9**, Suppl., 697 (1968).

[25] H. Neuhäuser and O. B. Arkan, *Phys. Status Solidi (a)* **100**, 441 (1987).

[26] H. Ney, R. Labusch and P. Haasen, *Acta metall.* **25**, 1257 (1977).

[27] H. Flor and H. Neuhäuser, *Res. Mech.* **5**, 101 (1982).

[28] T. Tanaka and H. Conrad, *Acta metall.* **19**, 1001 (1971).

[29] J. A. Gorman, D. S. Wood and T. Vreeland, Jr., *J. Appl. Phys.* **40**, 833 (1969).

[30] V. R. Parameswaran and J. Weertman, *Metall. Trans.* **2**, 1233 (1971).

[31] R. W. Guard, *Acta metall.* 9, 163 (1961).

[32] W. G. Johnston and D. F. Stein, *Acta metall.* **11**, 317 (1963).

[33] J. W. Christian, *Acta metall.* **12**, 99 (1964).

[34] G. M. Pharr and W. D. Nix, *Acta metall.* **27**, 433 (1979).

[35] J. T. Michalak, *Acta metall.* **13**, 213 (1965).

[36] T. H. Alden, *Acta metall.* **37**, 1683 (1989).

[37] T. H. Alden, *Mater. Sci. Engng* **A111**, 107 (1989).

[38] T. H. Alden, *Metall. Trans.* **18 A** 811 (1987).

[39] A. S. Keh, in *Electron Microscopy an Strength of Crystals*, G. Thomas and J. Washburn, (eds.), pp. 231-300, Interscience, New York-London (1963).

[40] J. D. Livingston, *Acta metall.* **10**, 229 (1962).

[41] J. E. Bailey and P. B. Hirsch, *Phil. Mag.* **5**, 485 (1960).

[42] J. P. Hirth and J. Lothe, *Theory of Dislocations*, Wiley (1982).

[43] G. Simmons and H. Wang, *Single Crystal Elastic Constants and Calculated Aggregate Properties*, MIT Press (1971).

[44] J. H. Holbrook, J. C. Swearengen and R. W. Rhode, in *Mechanical Testing for Deformation Model Development*, R. W. Rhode and J. C. Swearengen, (eds.), pp. 80-101, ASTM STP 765, ASTM Philadelphia, Pa (1982).

[45] T. H. Alden, *research in progress* (1992).

[46] W. H. Press, B. P. Flannery, S. A. Teukolsky and W. T. Vetterling, *Numerical Recipes*, Cambridge Univ. Press, Cambridge (1989).

[47] C. J. McMahon, Jr. (ed.), *Microplasticity*, Interscience, New York, pp. 121-144 (1968).

Appendix A

Hard Tensile Machine Calibrations

A.1 Calibration of Initial Specimen Gauge Length

It is implicit in the analysis of the displacement of the crosshead, e.g. Eq. [2.21], that all inelastic deformation is confined to an appropriate initial specimen gauge length, L_o. Since additional inelastic deformation may occur in the fillets, which are between the parallel gauge section and the shoulders of the grip section, L_o is treated as an operational gauge length, over which all inelastic strain between specimen shoulders is distributed giving a strain which is equal to the uniform strain measured within the parallel section; i.e.

$$L_o = \frac{\Delta L_t}{e_t}, \tag{A.35}$$

where ΔL_t is the shoulder–to–shoulder elongation and e_t is the uniform strain within the parallel section.

Determination of the operation length can be easily done with two extensometers, one used to measure ΔL_t and the other e_t. However, in order to measure the shoulder–to–shoulder elongation, the required 1.5 inch (3.8 cm) extensometer was not on hand. Instead, inelastic elongation was determined by measuring, with a travelling microscope, the displacement of a pair of lines scribed across the shoulders. Applying Eq. [A.35] would underestimate the value of ΔL_t; however, this value may be corrected by including an estimate of the elastic elongation. Two such calibrations were done at 10 % uniform strain giving values of $l_o = 2.85$ and 2.87 cm; thus, l_o is taken to be the average value of

2.86 cm.

A.2 Determination of Machine Stiffness Constant

Manipulation of the coupling equation (of which Eq. [2.23] is a modified form) can provide several techniques for the determination of the machine stiffness K. The technique used in this investigation is the *elastic loading* method which is a simple technique that relies upon a preyield determination of the specimen loading rate $\dot{P}$. With this method, the coupling equation is solved for the combined specimen-machine modulus C by making the appropriate substitutions for elastic loading; i.e. $\dot{\epsilon}_i = 0$ and $\sigma = q\dot{P}/A_o$ Thus,

$$C = gq\frac{l_o}{A_o}\frac{\dot{P}}{\dot{X}} \tag{A.36}$$

Then M and finally K are determined from the following equations,

$$\frac{1}{C} = \frac{1}{E} + \frac{1}{M} \tag{A.37}$$

and

$$M = gqM_o \tag{A.38}$$

$$K = A_oM_o/l_o \tag{A.39}$$

It is apparent that the determination of K requires knowledge of the elastic modulus of the specimen *a priori*, and an independent determination of the stretch ratios $g = l_t/l_o$ and $q = l_i/l_o$ (these definitions will be made apparent in Figure).

To the application of this technique, a specimen with initial area $A_o = 2.20$ mm^2 and effective gauge length $l_o = 2.86$ cm was initially prestrained to 3.128 cm total extension, about 8.8 % strain, and then unloaded as shown in Figure A.23(a). An extensometer with gauge length of 2.54 cm and calibrated to 15 % extension, was used to measure the specimen extension. This was done, so that upon reloading, a more characteristic value

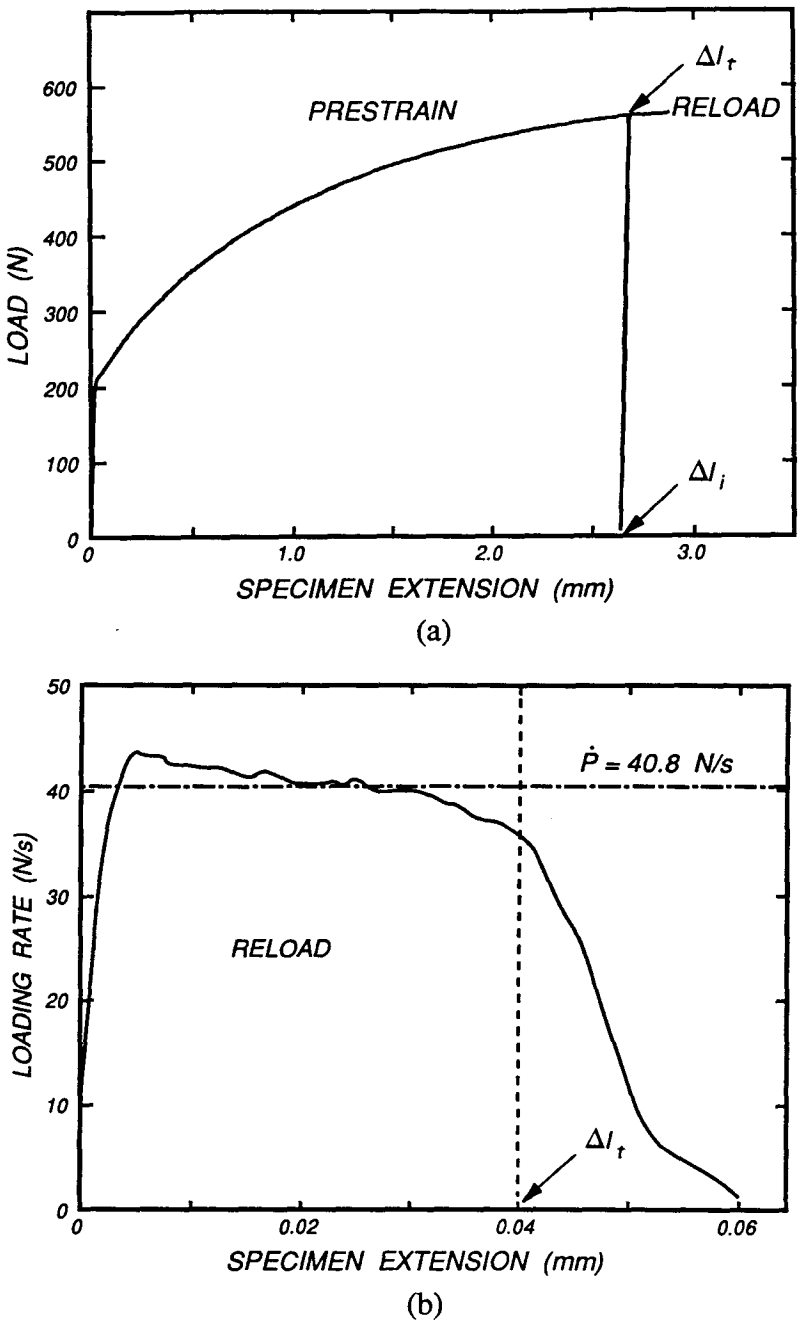

Figure A.23: Determination of the hard machine stiffness: (a) the total and inelastic elongations are determined from the load *vs* elongation curve for a specimen prestrained to 8.8 % uniform strain; and (b) the elastic loading rate is determined from the time derivative of the reloading curve *vs* specimen extension.

for $\dot{P}$ would be obtained for a larger load range. An average loading rate of 40.8 N/s for $\dot{X} = 8.47 \times 10^{-6}$ m/s (0.02 in/min) is indicated by the reloading curve shown in Figure A.23(b). K was determined to be 7.5 MN/m.